SLAC-PUB-3093
April 1983
(T/E)

e^+e^- INTERACTIONS AT VERY HIGH ENERGY: SEARCHING BEYOND THE STANDARD MODEL

JONATHAN DORFAN*
Stanford Linear Accelerator Center
Stanford University, Stanford, California 94305

Lectures Presented at the
SLAC Summer Institute on Particle Physics:
Physics at Very High Energies
Stanford, California
August 16-27, 1982

* Work supported by the Department of Energy, contract DE-AC03-76SF00515.

Table of Contents

1. Introduction

These lectures discuss e^+e^- interactions at very high energies with a particular emphasis on searching beyond the standard model which we take to be $SU(3)_{color} \wedge SU(2) \wedge U(1)$. The highest e^+e^- collision energy exploited to date is at PETRA where data have been taken at 38 GeV. We will consider energies above this to be the "very high energy" frontier. The lectures will begin with a review of the collision energies which will be available in the upgraded machines of today and the machines planned for tomorrow. Without going into great detail, we will define the essential elements of the standard model. We will remind ourselves that some of these essential elements have not yet been verified and that part of the task of searching beyond the standard model will involve experiments aimed at this verification. For if we find the standard model lacking, then clearly we are forced to find an alternative. So we will investigate how the higher energy e^+e^- collisions can be used to search for the top quark, the neutral Higgs scalar, provide true verification of the non-Abelian nature of QCD, etc.

Having done this we will look at tests of models involving simple extensions of the standard model. Models considered are those without a top quark, those with charged Higgs scalars, with multiple and/or composite vector bosons, with additional generations and possible alternative explanations for the PETRA three jet events which don't require gluon bremsstrahlung.

From the simple extensions of the standard model we will move to more radical alternatives, alternatives which have arisen from the unhappiness with the gauge hierarchy problem of the standard model. Technicolor, Supersymmetry and composite models will be discussed. In the final section we will summarize what the future holds in terms of the search beyond the standard model.

We will be considering many different theoretical models in these lectures. The descriptions of the models will intentionally be brief (and non-rigorous); the main emphasis will be on the experimental implications of these models.

2. The e^+e^- Machines of the Future

The e^+e^- storage rings have been invaluable tools for the discovery and study of new thresholds. The fourth quark flavor was discovered at SPEAR as was the third lepton family. The clean environment provided by the e^+e^- storage rings SPEAR and DORIS permitted detailed study of charm spectroscopy and provided a wide variety of tests all of which pointed to the fact that the τ was in fact a universal lepton. The bottom quark was not discovered in e^+e^- interactions. However the studies at DORIS and CESR have provided a wealth of information about the bottom quark. The PETRA and PEP storage rings were built with the hope of discovering the top quark. Alas, top has not yet shown itself and the present PETRA limits indicate that the top quark is more massive than 18.5 GeV/c^2. However PETRA did bring striking confirmation of QCD as evidenced by events containing hard gluon bremsstrahlung. Also clear evidence for the electroweak interaction is apparent in the muon pair asymmetry measurements, the magnitude of the asymmetry confirming the predictions of the Weinberg-Salam model. These are only a few of the striking examples of how fruitful the investment in e^+e^- machines has been. With new thresholds to be tested, what energy ranges in e^+e^- interactions will be available to the experimenters of the future? We will concern ourselves here mainly with the parameters of the machines – the physics opportunities which go with these machines will be discussed in later sections.

During the next few years, PETRA will undergo a continuous energy upgrade[1] in search of the elusive top quark. By the end of 1982, PETRA will have doubled its complement of rf and will achieve a maximum energy of 40 GeV. This will be followed by the addition of new accelerating structures which will provide for a maximum energy of 46 GeV. The latter upgrade should be completed by April 1983. If the top quark has a mass below 23 GeV/c^2, we should have evidence of this from PETRA before the end of 1983. Toponium will provide many important tests of the standard model aside from the obvious confirmation that there indeed exists a sixth flavor. This exciting prospect might not be too far off.

If toponium still eludes PETRA, DESY may choose to install superconducting rf cavities in PETRA which would give them a maximum energy of 60 GeV. Two tests[2] with two different superconducting cavities have been performed at PETRA. Both

tests were most promising – a $\sim$ 9 GeV beam of electrons was stored in PETRA using a single superconducting cavity. Certainly no decision has yet been made to continue beyond 46 GeV. However, the means to achieve energies of $\sim$ 60 GeV at PETRA appear in hand. The time scale for such an upgrade is not clear, but if DESY were committed, PETRA could be operating with superconducting rf by late 1985. Estimates of the luminosity at these higher energies are uncertain at this time.

A conventional e^+e^- storage ring, TRISTAN, utilizing warm rf is presently under construction at KEK in Japan. This machine fills the KEK site and will have a maximum energy of $\sim$ 60 GeV. The design luminosity for the machine is $4 \times 10^{31}\ cm^{-2}\ sec^{-1}$. The present schedule calls for turn-on in early 1986 with at least two of the four interaction regions instrumented with general purpose particle detectors. A more complete description of the project can be found in Ref. 3. If PETRA stops its upgrade at an energy of 46 GeV, the TRISTAN machine will cover the territory up to 60 GeV with good luminosity.

The next big jump in available energy will come with the completion of the Stanford Linear Collider (SLC) at SLAC. The present schedule shows the SLC delivering colliding beams in late 1986. The design luminosity of the machine is $6 \times 10^{30}\ cm^{-2}\ sec^{-1}$ and the maximum energy at turn-on will be 100 GeV. A complete description of the SLC can be found in Ref. 4. However, since the SLC is not a conventional e^+e^- storage ring, we provide here a short description of the machine referring to Fig. 1. The existing linac will be upgraded to 50 GeV using an extension of the SLED ideas which enabled SLAC to raise the linac energy from 22 GeV to 34 GeV. An electron bunch is diverted out of the linac and collided with a target to produce positrons. These positrons are then fed back into the front end of the accelerator. Following passage through damping rings, which provide cooling for the electron and positron bunches, a bunch of positrons immediately followed in the next linac bucket by a bunch of electrons, is transported down the accelerator to the colliding arcs. The positrons and electrons are switched to different arcs and are brought into collision by an elaborate system of optics, termed the final focus. Following the collision, the beams are dumped. So unlike a storage ring, the SLC operates as a single pass collider. The repetition rate of the linac is 180 Hz, many orders of magnitude less than that of typical storage rings. To produce a usable luminosity, this slow collision rate must be compensated for. This will be done using an intense electron gun capable of producing 5×10^{10}

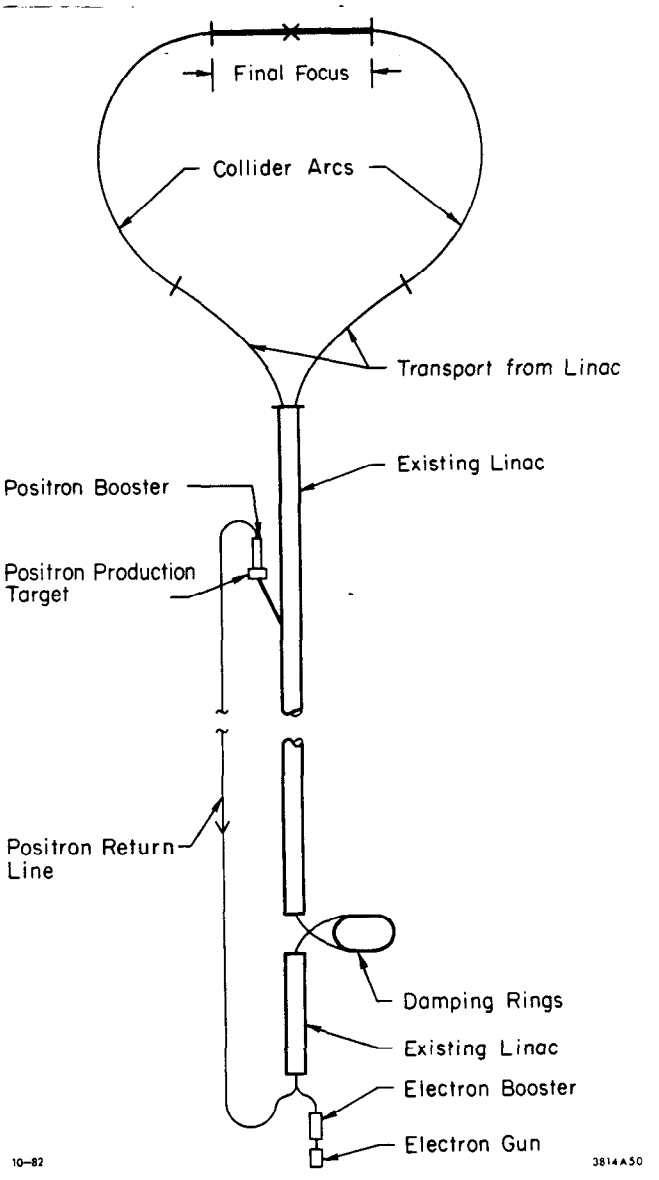

Fig. 1. Schematic layout of the SLC.

electrons per bunch and by designing the final focus optics such that the transverse dimensions of the colliding beams are a few microns as opposed to conventional storage rings where these dimensions are typically a few millimeters. The expected luminosity as a function of collision energy is shown in Fig. 2. The SLC is optimized to run at the Z^0. However, the luminosity remains good down to energies of 60 GeV. If toponium should be above TRISTAN, the SLC could, in principle, be used to study it. The SLC has the disadvantage of serving only one detector at a time.

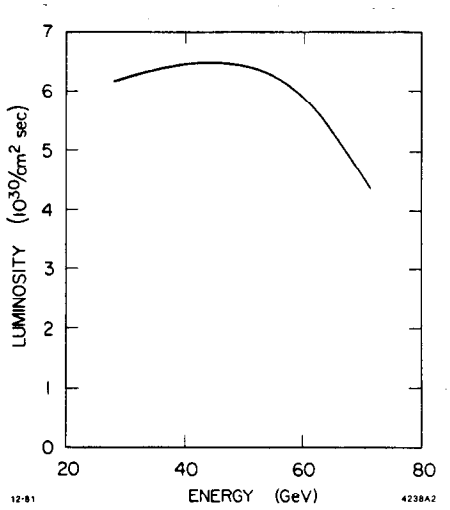

Fig. 2. Luminosity versus beam energy for the SLC.

The SLC project is an adventurous one to say the least. The linac must be upgraded to 50 GeV. High intensity, low emittance beams must be transmitted faithfully to the final focus which has the difficult task of focusing the beams down to micron spot sizes. It has the advantages of being cheap to build (M$ 100 for the machine) and will provide Z^0 physics in the very near future. Even at a luminosity of 10^{29} the SLC will be an interesting machine in 1987, providing $\sim$ 200 Z^0's per day. The physics goals of the SLC are clear – study the physics at the Z^0. In addition, the SLC is an important step into the future providing the first high energy test of the concept of linear colliders. The cost of a conventional storage ring goes like the square of the center of mass energy ($E_{c.m.}$), whereas the cost of a linear collider goes linearly with $E_{c.m.}$. It is entirely possible that LEP (see below), with its initial phase providing $E_{c.m.} = 100$ GeV at a cost $\sim$ M$ 500, will be the last frontier e^+e^- storage ring which we can afford to build.

Another feature of the SLC is the promise of longitudinally polarized beams, which are a powerful tool for the study of Z^0 physics.[5] Polarized electrons are produced by shining circularly polarized laser light on a galium arsinide cathode. Such an electron gun exists and has been successfully tested. Polarized electrons have already been transported down the linac and simulations of transport through the SLC arcs indicate that the transmission efficiency for the polarized electrons is $\geq 80\%$. The sign of the

laser polarization can be reversed on a linac pulse by pulse basis yielding successive beam pulses of opposite spins. Hence it appears that, with very high probability, beams with polarizations of $\geq 50\%$ will be available at the SLC.

If the linac could be raised beyond the 50 GeV beam energy, a second phase of the SLC will be possible providing maximum collision energies of $\sim$ 140 GeV.

While the U.S. high energy e^+e^- program is putting its money into the SLC, the European program for very high energies centers around the LEP project. LEP is a conventional e^+e^- storage ring which will be built at CERN. In its first incarnation – which we term LEP I – it will achieve a maximum collision energy of 100 GeV and a luminosity of 10^{31}. The project[6] is vast – requiring a tunnel with a 27 Km circumference – but the machine uses conventional storage ring technology and hence one should feel fairly confident that the design goals will be met. LEP I is slated for turn-on in about the middle of 1988 at a cost of $\sim$ M$ 500. LEP will have eight experimental halls of which four will be instrumented for LEP I.

The strength of the LEP program resides in its potential to go to $\leq$ 250 GeV collision energies. This is achieved in two different steps. By the addition of conventional rf, the machine will yield a maximum collision energy of 170 GeV (LEP II). By the application of superconducting rf the machine can go to $E_{c.m.} \leq 250$ GeV depending on the accelerating gradient which is achieved (LEP III). Gradients of 3 MeV/m, corresponding to $E_{c.m.} = 220$ GeV, have already been achieved in the PETRA tests.[2] The parameters of these two routes are summarized in Table 1. Time scales and costs for these upgrades are not known yet. As a guess LEP II could be available in early 1990. Beam polarization at LEP is much less certain than at SLC. A considerable amount of work is being done in this area, but there are still many hurdles to cross. These hurdles are discussed in Ref. 7.

Conceptual designs for very high energy colliding linacs exist both at SLAC and NOVOSIBIRSK. The Russian VLEPP project is described in detail in Ref. 8. The motivation for linear colliders was stated earlier, namely the cost grows linearly with $E_{c.m.}$ whereas the cost of circular machines grows as $E^2_{c.m.}$. Taking into account the constants of these equations, one finds that the crossover point is roughly at $E_{c.m.} =$ 150 GeV. This assumes of course, that in both cases one starts from scratch. Hence

Table 1. Summary of LEP Performance With Room-Temperature rf.

	1/6 of rf installed	1/4 of rf installed	1/2 of rf installed	1 rf installed
Installed rf power (MW)	16	24	48	96
Length of rf structure (m)	271.5	407.2	814.4	1628.8
Number of experiment areas with rf	2 (partial)	2 (full)	4 (full)	8 (full)
Maximum energy (zero luminosity) (GeV)	59.0	65.5	78.0	93.0
Maximum current required (mA)	2.8	3.1	3.8	4.7
Maximum luminosity ($\Delta Q = 0.03$) ($\times 10^{31}\ cm^{-2}\ sec^{-1}$)	0.9	1.3	1.8	2.7
Energy of maximum luminosity (GeV)	51.5	58.5	70.0	85.0

LEP Maximum Energies With Superconducting rf.

Maximum accelerating gradient (MV/m)	Two experiment areas with rf $L_c = 407.2m$	Four experiment areas with rf $L_c = 814.4m$	Eight experiment areas with rf $L_c = 1628.8m$
2.0	70.3	83.6	99.4
3.0	77.8	92.5	110.0
4.0	83.6	99.4	118.2
5.0	88.4	105.2	125.0

it would seem that to go substantially beyond the energy of LEP III, one will require a colliding linac machine. The general consensus seems to be to build a first phase machine capable of 300-500 GeV collision energy followed by a second phase in the $\geq$ 1 TeV range. Much will depend on what is learned from the SLC. In addition luminosities of $\geq 10^{32}$ are needed to test current ideas at the $\geq$300 GeV energy scale. I include this terse discussion here to emphasize that the intellectual effort and research

and development is going on in many areas so that the door to e^+e^- collisions in the 1 TeV region may be opened in the 1990's.

This section concludes with Table 2 which summarizes the machine possibilities for e^+e^- collisions for the foreseeable future.

Table 2. The e^+e^- Machines of the Future.

Where	When	$E_{c.m.}^{max}$ (GeV)	$\mathcal{L}_{design}^{max}$ $(cm^{-2}sec^{-1})$
PETRA, DESY	October 1982	40	1.5×10^{31}
PETRA, DESY	April 1983	46	$\sim 1.5 \times 10^{31}$
PETRA, DESY	?; by late 1985?	60	?
TRISTAN, KEK	January 1986	60	4×10^{31}
SLC I	October 1986	100	6×10^{30}
SLC II	?	140	4×10^{30}
LEP I	June 1988	100	10^{31}
LEP II	?	170	3×10^{31}
LEP III	?	220-250	?
VLEPP I	1990's	300	10^{32}
VLEPP II	?	1000	10^{32}

3. The Standard Model

We take $SU(3)_{color} \wedge SU(2) \wedge U(1)$ as the standard model. To describe this model in detail goes way beyond the scope of these lectures. Instead we need to characterize the main features of the model so that we can catalogue those features which are still not verified. No attempt has been made here to be complete or rigorous; rather we have in mind compiling, in as brief a manner as possible, the list of essential elements which will appear at the end of this section.

The class of "locally gauge invariant theories" form the theoretical framework for the standard model. Since their use is so pervasive, we will take some time to remind ourselves of the terminology. We use the $U(1)$ gauge group of electromagnetism as an example.

Consider the matter field of an electron. If we change the phase of the field by the same amount in all space we will find that the physics remains invariant. The reason for this is clear – the physics is determined by differences in phases and the global transformation discussed above will leave all phase differences fixed. We say that the electron matter field is "globally gauge invariant" with respect to phase rotations. Suppose, however, that we perform a local gauge transformation, namely we change the phase at one point in space only. Clearly this will change all relative phases and hence all physical measurables. To preserve the local symmetry we must add an additional new field, which is designed to compensate over all space for the local disturbance. As is well known to the reader, one adds to the free electron matter field a vector field whose quantum is the photon. Since compensation for the local disturbance is required over infinite distances, the photon must be massless. The order of successive local gauge transformations (successive photon emissions from an electron for instance) does not affect the physics since, in all cases, the phase change resulting from the transformations is the same. Because successive transformations commute, the theory – namely QED – is termed Abelian and the reason that QED is Abelian is that the photon does not carry the property which is conserved, that is the photon is "chargeless." To summarize, QED is a locally gauge invariant Abelian theory, and the local gauge invariance was ensured by the addition of a new field.

By direct analogy with QED, $SU(3)_{color}$ is described by a locally gauge invariant theory. The conserved quantity is color. In the standard model quarks come in six flavors – u, d, s, c, b and t – and each quark has three color degrees of freedom. Since hadrons do not exhibit color, they are color singlets. Baryons are composed of three quarks and mesons of a quark anti-quark pair. In QCD local gauge invariance is ensured by the addition of sixteen fields. The quanta of these fields are eight gluons most of which, in order to preserve the local gauge invariance, must carry color. In general, successive local gauge transformations (successive emissions of gluons from a quark for instance) will not commute because the gluons carry color. Hence QCD is a non-Abelian theory. The non-Abelian nature of QCD has some important experimental consequences.

In QED the vacuum becomes polarized by the presence of virtual e^+e^- pairs, which leads to the screening of bare electric charge. In QCD the vacuum contains both virtual quark pairs and virtual gluon pairs. This combination conspires to anti-screen bare color charge. This leads to the notion of asymptotic freedom and the accompanying features that (a) quarks and gluons are confined by the color field (i.e., we should not see free quarks) and (b) the strength of the strong (color) coupling constant, α_s, depends on the distance scale of the probe. The notion of a running coupling constant is expressed, to leading order in logs, as

$$\frac{1}{\alpha_s(Q^2)} = \frac{1}{\alpha_s(q^2)} + \frac{32 - n_f}{12\pi} \; log\left(\frac{Q^2}{q^2}\right)$$

where n_f is the number of quark flavors.

Since the gluons carry color, they can couple to themselves as well as coupling to a quark anti-quark pair. This self coupling is a consequence of the non-Abelian nature of QCD and hence any evidence for this self coupling constitutes a test of this very important feature of QCD. (Notice that there is no analog of the gluon self-coupling in QED.)

Consider Fig. 3 in which (a) a gluon is shown emitting a gluon and (b) a quark is shown emitting a gluon. If the parton energies are high enough, then this perturbative picture makes sense and one finds that the probability for 3(a) is 9/4's larger than for 3(b). The fact that the gluon-gluon coupling is about twice as probable as the quark-gluon coupling implies that gluons should fragment to roughly twice as many

hadrons as quarks of the same energy. The average transverse momentum of the decay products should also be different for quark and gluon jets. This QCD prediction holds only if you believe the perturbative picture described above. In all likelihood this picture is sound and we will treat this fragmentation difference between quarks and gluons as an important prediction of QCD.

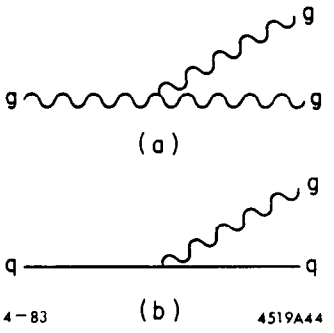

Fig. 3. The perturbative representation of the processes whereby a gluon radiates a gluon (a) and a quark radiates a gluon (b).

In the standard model, leptons are point-like particles which carry no color. Hence they are unaffected by the strong interaction. They couple to the gauge bosons of $SU(2)$ through their weak charge (helicity) and to the photon of $U(1)$ through their electric charge. There are six leptons — $e, \mu, \tau, \nu_e, \nu_\mu$ and ν_τ. The left-handed fermions of $SU(2)$ are arranged in flavor conserving doublets:

$$\begin{pmatrix}\nu_e\\ e\end{pmatrix}_L \qquad \begin{pmatrix}\nu_\mu\\ \mu\end{pmatrix}_L \qquad \begin{pmatrix}\nu_\tau\\ \tau\end{pmatrix}_L$$

$$\begin{pmatrix}u\\ d'\end{pmatrix}_L \qquad \begin{pmatrix}c\\ s'\end{pmatrix}_L \qquad \begin{pmatrix}t\\ b'\end{pmatrix}$$

The primes on the quarks indicate that the flavor conservation in the quark sector is not perfect. This generation mixing is summarized by the elements of the Kobayashi-Maskawa matrix, the most familiar component of this matrix being the Cabibbo angle which tells us that the d quark has a 5% strange quark admixture. The right-handed fermions occur in singlets u_R, d_R, s_R, c_R, b_R, t_R, e_R, μ_R and τ_R. In the standard model we have three generations. Associated with each charged lepton is a neutral, massless lepton. Since the neutrinos have identically zero mass, there are no right-handed neutrinos.

We have now specified the particles of $SU(2) \wedge U(1)$. At this time it is a gauge invariant — with respect to weak isospin — theory with four massless bosons. This is

problematical because (a) we have too many massless (long range) fields and (b) the local weak isospin symmetry implies that fermions are massless. Enter the cunning of the Higgs mechanism which is used to spontaneously break the symmetry. In this scheme, while the Lagrangian of the theory remains invariant, the vacuum (ground state) does not. The fact that the vacuum is not invariant implies that there exists stored energy in the vacuum. This stored energy is used to give mass to the bosons and the charged fermions. In the standard model the minimal Higgs scheme is used to spontaneously break the symmetry. This is achieved using a doublet of complex fields:

$$\phi = \begin{pmatrix} \phi^+ \\ \phi^0 \end{pmatrix}$$

$$\phi^+ = \phi_1^+ + i\phi_2^+$$

$$\phi^0 = \phi_1^0 + i\phi_2^0 \quad .$$

We add a term to the Lagrangian:

$$\mathcal{L}_{Higgs} = T_{Higgs} - V_{Higgs}$$

where $V_{Higgs} = -\frac{|u^2|}{2}\,\phi^+\phi + \frac{|\lambda|}{4}\,(\phi^+\phi)^2$. If $u^2 > 0$, one finds the vacuum expectation value of ϕ is $< \phi >_0 = \begin{pmatrix} 0 \\ V \end{pmatrix}$ where $V^2 = \frac{|u^2|}{\lambda}$. When the symmetry is broken, three of the boson fields acquire mass, eliminating three of the Higgs fields. These massive bosons are the familiar $W^\pm$ and Z^0. The fourth Higgs field remains as a physical scalar particle – the neutral Higgs particle H^0. The mass of the H^0 is given by $M_{H^0} = 2|u^2| = 2\lambda V^2$. Since the theory does not specify λ we have no prediction for the Higgs mass. However, we do get some guidance from theory which indicates that $7.5 \leq M_{H^0} \leq 10^3$ GeV/c^2. The lower limit comes about from considering $u^2 \equiv 0$ with the symmetry breaking arising purely from radiative corrections. A very massive H^0 is not likely when the mass scale which it is generating is $\sim$ 100 GeV/c^2. The lack of a crisp prediction for the H^0 mass, makes searching for the H^0 very difficult indeed. Fermion masses are generated by Yukawa couplings of the Higgs field. An interaction term is added to the Lagrangian:

$$\mathcal{L}_{int} = -\mathcal{G}\{\bar{R}\phi^+ L + \bar{L}\phi^+ R\} \quad .$$

In $SU(2) \wedge U(1)$ the two neutral quanta are not the physically observed particles. Rather the photon and the Z^0 are orthogonal admixtures of these neutral quanta with the relative amount of mixing specified by the Weinberg angle, θ_W. In terms of this angle, one obtains predictions for the $W^{\pm}$ and Z^0 masses:

$$M_W^2 = \frac{\pi\alpha}{\sqrt{2}\,\mathcal{G}_F} sin^2\theta_W \tag{1}$$

$$M_{Z^0}^2 = M_W^2/cos^2\theta_W \tag{2}$$

where α is the fine structure constant and $\mathcal{G}_F$ is the Fermi coupling constant.

The quantity $sin^2\theta_W$ has been measured in many different experiments and Kim et al[9] derive an average of 0.23 ± 0.015. One cannot use this value directly in Eqs. (1) and (2) to yield the boson masses because of the effects of radiative corrections. The bare mixing angle of the theory is given by $sin^2\theta_W^0 = \frac{e^2}{g^2}$ where e and g are the $U(1)$ and $SU(2)$ coupling strengths. The renormalized, physically measurable $sin^2\theta_W^R$ is related to $sin^2\theta_W^0$ by a radiative expansion:

$$sin^2\theta_W^0 = sin^2\theta_W^R\left(1 - \frac{\alpha}{\pi} f(sin^2\theta_W^R) + O(\alpha^2)\ldots\right) .$$

Marciano and Sirlin have studied this problem[10] and find that $sin^2\theta_W^0$ is roughly 7% larger than the measured value. Hence they predict

$$M_W = (82 \pm 2.4)GeV$$

$$M_{Z^0} = (93.0 \pm 2.0)GeV \quad .$$

Notice that a precise measurement of M_{Z^0} and an independent measurement of $sin^2\theta_W$ permit one to test the validity of the radiative correction calculations. We will see later that this can be done.

In the standard model the weak left- and right-handed fermion couplings are specified by $g_{L,R} = T_3^{L,R} - Q\ sin^2\theta_W$ where Q is the fermion charge and T_3 is the third component of the weak isospin. A more commonly used notation is

$$g = \frac{(g_R + g_L)}{2}$$

$$a = \frac{(g_R - g_L)}{2} \quad .$$

Table 3 summarizes these values for the fermions of the standard model assuming $sin^2\theta_W = 0.23$.

Table 3. Vector and Axial-Vector Fermion Couplings

Fermion	Axial Vector	Vector
ν	-0.25	0.25
e, μ, τ	0.25	$\frac{1}{4}(-1 + 4sin^2\theta_W) = -0.02$
u, c, t	-0.25	$\frac{1}{4}(1 - \frac{8}{3}sin^2\theta_W) = 0.10$
d, s, b	0.25	$\frac{1}{4}(-1 + \frac{4}{3}sin^2\theta_W) = -0.17$

The coupling of the neutral Higgs to a pair of fermions is given by

$$g_{H^0 f\bar{f}} = 2^{\frac{1}{4}}\sqrt{\mathcal{G}_F}\, M_f$$

$$\simeq 3.8\left(\frac{M_f}{M_p}\right)10^{-3}$$

where M_f and M_p are the fermion and proton masses. The important thing to notice is that the H^0 will couple to pairs of the heaviest fermions available. This fact will be used in searches for the H^0. The Higgs coupling to bosons is given by

$$g_{H^0 V\bar{V}} = 2^{\frac{5}{4}}\sqrt{\mathcal{G}_F}\, M_V^2$$

$$\simeq 7.6\left(\frac{M_V^2}{M_p^2}\right)10^{-3}$$

where M_V is the boson mass. So while the standard model does not predict masses for the fermions and the H^0, it does specify the couplings.

We have now covered sufficient ground to arrive at the catalog of characteristics which we will need to discuss high energy tests of the standard model.

1. The fundamental fermions are six quarks and six leptons: u, d, s, c, b, t, and $e, \nu_e, \mu, \nu_\mu, \tau, \nu_\tau$.
2. There are nine massless bosons: eight colored gluons and the photon.
3. There are three massive vector bosons: Z^0, W^+, W^-.

4. There is one neutral scalar: H^0.

5. QCD is non-Abelian and hence: (a) particles which carry color are confined; (b) gluons couple to gluons; (c) the strong coupling constant, α_s, runs.

As we contemplate this catalog we realize that the t quark and the ν_τ have not been seen, we should review the evidence for the existence of gluons, none of the heavy vector bosons have been seen, the H^0 has not been seen and there is no evidence for the essential feature of QCD – namely that it is a non-Abelian theory.

Before we embark upon considering to remedy these untested features using high energy e^+e^- interactions, we should remember that the standard model, both QCD and the electroweak sector, is an outstanding success at low energies. There is considerable verification from all areas of experimentation and there exist no well established conflicts with any experimental data. There is no reason then, aside from aesthetics like the unhappiness surrounding procedures like the Higgs mechanism, to expect that the standard model is an incorrect description of nature. We will have the means in the next few years to make many interesting and important high energy tests. And, as ususal, e^+e^- collisions will play a major role in these tests.

4. Testing the Standard Model in e^+e^- at Energies Beyond Those Currently Available

4.1 SEARCHING FOR THE TOP QUARK

The charge two-thirds top quark has not yet been seen. There is indirect evidence (see Sec. 5.3) from the absence of flavor changing neutral currents that there must be a top quark at some mass. There exists only one rather perverse "topless" model which has not been ruled out. It is then fairly certain that the top quark exists.

The present limits coming from PETRA are that the top quark mass, M_t, is below 18.8 GeV. These limits are set using either event shapes, high transverse momentum leptons arising from weak decays of heavy quarks or measurements of R the ratio of the hadronic cross section to the muon pair cross section.

In anology with the ψ and Υ systems, one expects to see several $t\bar{t}$ bound states below the threshold for open top. Energy scans have been done at PETRA to search for the $1S$ (toponium) state. Using $\sim$ 20 MeV energy steps, the energy ranges (a) 27 $< E_{c.m.} <$ 31.6 GeV and 33 $< E_{c.m.} <$ 37 GeV have been exhaustively scanned. For each scan point, R is determined. To get an upper bound on the width of a possible $t\bar{t}$ bound state, each measured point is fitted to a Gaussian plus a constant term. Radiative effects are also included in the fits and the width of the Gaussian is taken to be the machine energy resolution of 20 MeV. The resonance parameters are related to the data via

$$\int \sigma_{tot}(E_{c.m.}) d\, E_{c.m.} = \frac{6\pi^2}{m^2_{t\bar{t}}} \Gamma_{ee} B_{had}$$

where $M_{t\bar{t}}$ is the assumed resonance mass, Γ_{ee} the partial width for the decay to electrons and B_{had} is the hadronic branching fraction. Fig. 4 shows the combined data from the four PETRA experiments of JADE, MARK J, CELLO and TASSO. Table 4 shows the values of $M_{t\bar{t}}$ where the fit yields a maximum $\Gamma_{ee}\, B_{had}$ for each individual experiment and for the combined data ($M_{t\bar{t}} = 33.34$ GeV) for which $\Gamma_{ee}\, B_{had} < 0.61$ keV (90% confidence limit).

Table 4. Results of the $t\bar{t}$-Resonance Search

Experiment	Mass of the Assumed Resonance GeV	Upper Limit of Electronic Width × BR(hadrons) keV (90% C.L.)
CELLO	33.52	1.79
JADE	33.34	1.22
MARK J	35.12	0.97
TASSO	33.34	1.33
All Experiments	33.34	< 0.61

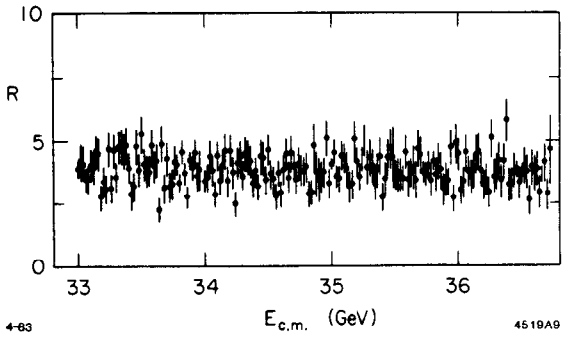

Fig. 4. $R = \sigma_{hadrons}/\sigma_{\mu\mu}$ in the region of the PETRA toponium energy scan. The data of all experiments (CELLO, JADE, MARK J and TASSO) are combined.

All $q\bar{q}$ resonances ($\rho, \omega, \phi, \psi, \Upsilon$) have the common feature that $\frac{\Gamma_{ee}}{e^2} \sim 10$ keV where e is the quark charge. If we assume that this is true for the $t\bar{t}$ system and that $B_{had} \geq 0.7$ then one would expect $\Gamma_{ee}\, B_{had} > 3$ keV for toponium. Thus the PETRA data rule out the existence of toponium up to a mass of 37 GeV/c^2.

The PETRA measurement of R has also been used to demonstrate that the open top threshold has not yet been reached.[13] In the simple quark parton model R is given by

$$R = \frac{\sigma_{had}}{\sigma_{\mu\mu}} = 3\sum_i e_i^2$$

where e_i are the quark charges and i runs over the flavors which are below threshold. For the five known flavors, $R = 3.67$ in this model. There are small modifications to the simple picture from QCD of the order of π/α_s. The prediction[14] of QCD for five flavors is $R = 3.88$ and for the inclusion of a sixth charged two-thirds flavor $R = 5.31$.

Averaging over $E_{c.m.}$ from 12 to 37.6 GeV, a value of $< R >= 3.84 \pm 0.04$ is obtained from the PETRA data. This error is statistical only and to be conservative a 10% systematic error should be assigned to $< R >$. Clearly the PETRA data rule out open top production up to 37.6 GeV.

The standard model does not calculate fermion masses and so the absence of the t quark does not imply an essential problem. Box diagrams would contribute to the $K_L - K_S$ mass difference and the decay rate for $K_L \rightarrow \mu^+\mu^-$. Buras,[11] using such an approach, consoles us with the bound that $M_t \leq 40$ GeV. What prospects exist for finding the top quark?

As we have seen, the most straightforward way of looking for top is to measure R. If one assumes one is above the top threshold then a $\delta_R = 4/3$ should be seen. If we require a 3σ effect in R, we must measure to an accuracy $\sigma_R/R \simeq 8\%$. Typical PEP and PETRA experiments achieve $\leq 5\%$ for the systematic contribution to the error in the measurement of R and we will ignore these in this discussion. Allowing for statistical errors in both the luminosity measurement and the counting of hadrons, $\sigma_R/R = 8\%$ requires a sample of ~ 200 hadronic events. If N is the number of days to accumulate M hadronic events in a detector with an efficiency of ϵ, then

$$N = \frac{E^2_{c.m.} \times 10^{33}}{86.8R < \mathcal{L} > \epsilon(3.6 \times 24 \times 10^3)}$$

where $E_{c.m.}$ is in GeV and $< \mathcal{L} >$ is the average luminosity measured in units of $cm^{-2}\ sec^{-1}$. Typically $\epsilon = 0.7$ and referring to Table 2, $< \mathcal{L} >$ can be taken as $5 \times 10^{30} cm^{-2}\ sec^{-1}$. One finds then

$E_{c.m.}$ (GeV) $(= 2M_t)$	Who, When	Number of Days for $\sim 10\%$ Measurement of R
41	PETRA, December 1982	2.5
45	PETRA, June 1982	3.0
60	TRISTAN, March 1986	5.0

Hence the measurement of R is a fast way of finding top if one is above the open top threshold. If the results of this search are negative, then one can begin scanning down in energy looking for the $1S$ state. This state will be narrower than the machine width which is 20 MeV at PETRA and projected to be 60 MeV at TRISTAN. One scans therefore in steps comparable to the machine energy. As an example of how long such a scan would take, consider Fig. 5 which is the hadronic cross section (see Ref. 3) expected at TRISTAN given that toponium is at 50 GeV. The toponium resonance has been corrected for radiative effects and the beam energy spread. Remembering that one would scan in $\sim$ 60 MeV steps, one sees that almost independently of one's initial choice of energy for the scan, one will reach a scan point within 90% of the best possible resonant yield. The non-resonant cross section is approximately equal to this resonant yield and therefore one would run long enough to see $\sim$ 25 events in the continuum. The on-resonance response would then be 50 events, and one would have a significant effect with these statistics. At $< \mathcal{L} >= 5 \times 10^{30} cm^{-2}\ sec^{-1}$ it takes ten hours to accumulate 25 events at a cross section of $\sigma = .15nb$. Hence one could scan at a rate of 1 GeV/week. Having established that one was not above open top threshold first, one would then scan down from this energy, E_0. If the $1S$ state were not found within $\sim$ 4 GeV below E_0 – four weeks running – then in all probability top will be at an energy above E_0. Clearly we have not chosen the best optimization strategy here since adjacent points in the scan can be added together. But the flavor of the discussion is correct – it would take several weeks of scanning to look for hidden top at TRISTAN given that open top was not at the maximum machine energy. For PETRA the number of events required to establish toponium is about the same. However, here the machine width is smaller and the luminosity uncertain. By the time these lectures are published, the scan rate for PETRA will have been established. I would guess that it will take about twelve hours per 20 MeV step.

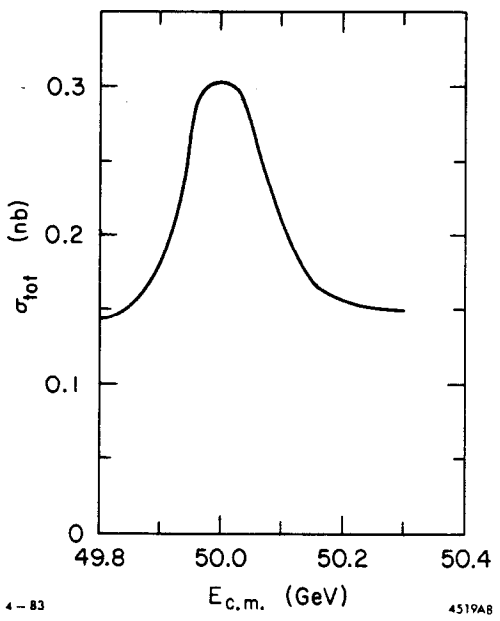

Fig. 5. The hadronic cross section in the region of 50 GeV assuming toponium is at a mass of 50 GeV.

If M_t >30 GeV, then the next place to look in e^+e^- collisions will be the SLC and soon thereafter LEP. A shape analysis of the hadronic events or the yield of large transverse momentum (with respect to the thrust axis) leptons will be a very clean and rapid signal for top at the Z^0. These tests are discussed fully in SLAC REPORT 247 (see Ref. 5b). Figure 6 shows the yield of events as a function of the aplanarity for the t quark and separately for the five lighter quarks. A 30 GeV/c^2 mass was assumed for the t quark. The curves are normalized to a one-week run at the SLC assuming $< \mathcal{L} >= 3 \times 10^{29}\ cm^{-2}\ sec^{-1}$. The aplanarity[12] measures the amount of momentum out of the event plane as it is defined in a sphericity analysis. As the t quark mass is raised, the mean aplanarity for the t quark grows. A short run at the SLC would readily establish the presence of a t quark if M_t >30 GeV/c^2. Figure 7 shows the transverse momentum of muons, relative to the produced quark direction, for different quark parents. The top quark mass was assumed to be 25 GeV/c^2. A clear separation between top and all other species is seen. So if 30 GeV < M_t < $M_{Z^0}/2$ the SLC and/or LEP will easily find top.

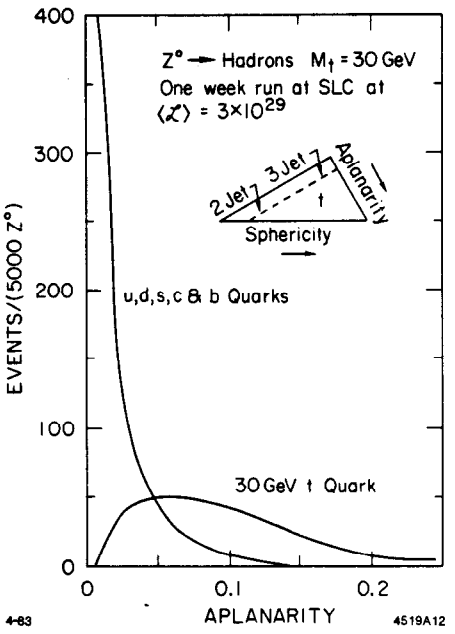

Fig. 6. The aplanarity distribution for events of the type $Z^0 \rightarrow q\bar{q}$. The distribution for $Z^0 \rightarrow t\bar{t}(M_t = 30\ \mathrm{GeV/c^2})$ is shown separately from the lighter quarks.

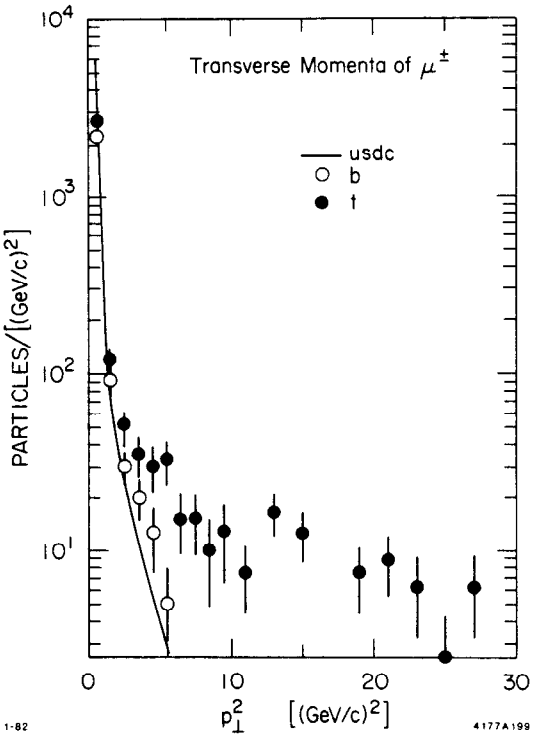

Fig. 7. The distribution of transverse momentum squared, with respect to the quark direction for all muons in the event. Contributions from the different flavors are indicated in the figure.

How is the top quark mass measured at the Z^0? The aplanarity distribution and the lepton transverse momentum distributions are strongly dependent on M_t.

Certainly a rough estimate (probably $\pm$ 5 GeV/c^2) would result from such distributions but the result would depend strongly on the Monte Carlo assumptions for t quark fragmentation, etc. The jet mass does not prove to be a reliable measure of M_t. The jet mass distributions for t quark events selected by a cluster analysis[15] and aplanarity cuts appears in Fig. 8. The cluster algorithm in conjunction with an aplanarity cut $\geq$ 0.04 yielded, in this study, a $Z^0 \rightarrow t\bar{t}$ event sample with 80% purity (see Ref. 5b, pages 93-100). For M_t = 19 GeV/c^2 (Fig. 8a) the mean jet mass is about 16 GeV/c^2. For M_t = 30 GeV/c^2 (Fig. 8b) the mean jet mass increases to only 19 GeV/c^2. Thus the measured jet invariant mass is not linear in M_t; the nonlinearity becomes most marked for $M_t \geq$ 20 GeV/c^2. The reason for this behavior is that as M_t increases the events become more spherical and the assignment of the numerous soft particles to the jets becomes somewhat arbitrary: the jets are not distinct clusterings of particles. The determination of M_t from jet masses appears too dependent on Monte Carlo simulations to be of much use.

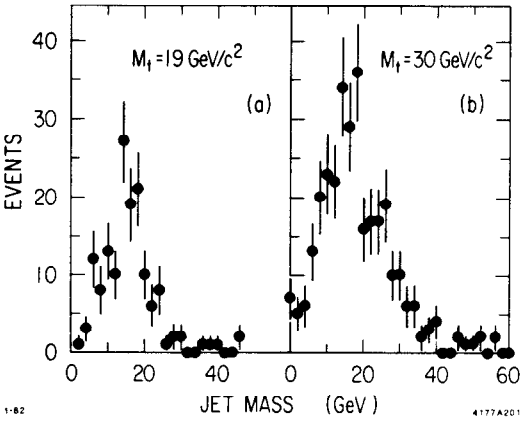

Fig. 8. The reconstructed jet masses for two-cluster events with aplanarity $\geq$ 0.04 for (a) top quark mass M_t = 19 GeV/c^2 and (b) M_t = 30 GeV/c^2.

A more promising method[16] does not depend at all on the Monte Carlo simulation of the fragmentation process, but on the rate of hadron production at the Z^0. It is based on the fact that in the standard electroweak theory the partial width for $Z^0 \rightarrow t\bar{t}$ is given by

$$\Gamma_t(\beta) = 3\left(\frac{M_{Z^0}}{24\pi}\right)[g_V^2\ \beta(3-\beta^2) + 2g_A^2\ \beta^3]\ .$$

where β is the t velocity in units of the speed of light, and g_A and g_V are the t quark weak axial-vector and vector couplings, function of $sin^2\theta_W$ only. For $sin^2\theta_W$ = 0.23,

$g_A^2 \gg g_V^2$ and the threshold factor for $Z^0 \rightarrow t\bar{t}$ is predominantly cubic in β. Hence the rate for $Z^0 \rightarrow t\bar{t}$ is strongly modulated by the threshold factor, and the overall rate for $Z^0 \rightarrow$ *hadrons* is correspondingly reduced by the t mass effects provided $M_t < M_{Z^0}/2$. Figure 9 shows the ratio

$$\rho = \frac{\Gamma_t(\beta)}{\Gamma_u}$$

as a function of the t quark mass. Here Γ_u is the partial width for $Z^0 \rightarrow u\bar{u}$ (i.e., $Z^0 \rightarrow$ *massless* $Q = \frac{2}{3}$ *quarks*). With the present lower bound on M_t of 18.5 GeV, there would be 22% less hadrons from massive $t\bar{t}$ production than from massless t quarks. Since 14% of $Z^0 \rightarrow$ *hadrons* is in the $u\bar{u}$ channel, an overall reduction of 3% of the hadronic rate is expected for $M_t = 19$ GeV/c^2 as compared to $M_t = 0$.

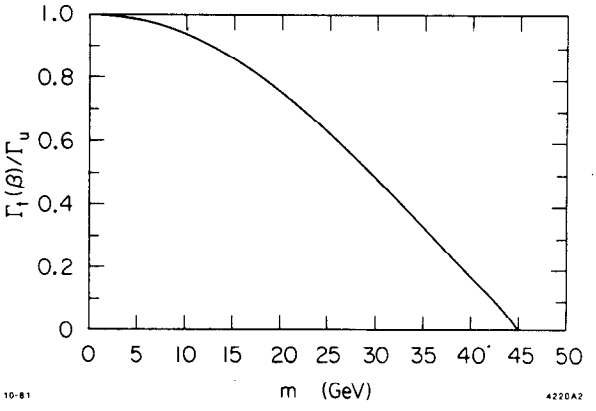

Fig. 9. The suppression factor of $t\bar{t}$ decays of the Z^0 as a function of the top quark mass for $sin^2\theta_W = 0.22$ and $M_{Z^0} = 90$ GeV/c^2.

Within the standard model ρ can be expressed in terms of the ratio r of the number of hadronic events (N_h) to the number of muon pair events ($N_{\mu\mu}$) produced at the Z^0:

$$\rho = 1 + r\,\frac{\Gamma_{\mu\mu}}{\Gamma_u} - \frac{\Gamma_h}{\Gamma_u}\,,$$

where Γ_h is the hadronic width calculated for three quark generations of massless, colored weak isospin doublets, $\Gamma_{\mu\mu}$ is the calculated $\mu^+\mu^-$ partial width and Γ_u is the calculated partial width into u quarks. Hence, in principle, the experiment is simple: it consists of counting the number of hadronic and muon pair events. There is no need to measure the luminosity, and the error of the t mass estimate depends on the ability of counting hadron events and muon pairs with small systematic errors. If one

assumes 10^6 Z^0's, $N_{\mu^+\mu^-} = 31{,}000$, $N_h = 730{,}000$ and $\delta(sin^2\theta_W) = 0.001$,[17] the t quark mass resolution, in the absence of any systematic error, is given in Fig. 10. The resolution is adequate and independent of t quark mass. Inevitably, there will be some systematic effects; the resolution degrades by $\sim$ 1 GeV per 1% systematic error in r. It should be pointed out that to apply this method one needs independent evidence that (a) the $t\bar{t}$ events are being produced at the Z^0 and (b) that there are no processes contributing to N_h beyond those of five known quarks. Nonetheless, this method looks very promising for estimating the t quark mass.

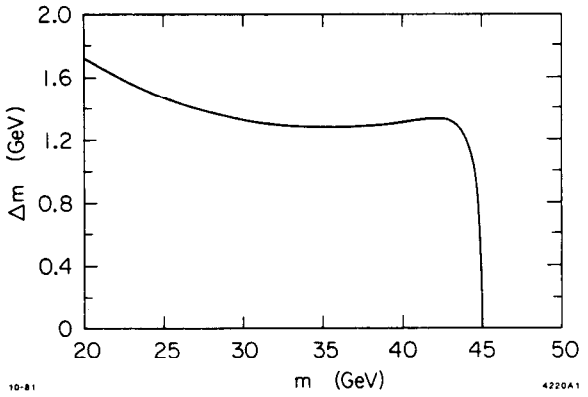

Fig. 10. The error in the determination of the top quark mass as a function of the top quark mass for a sample of $10^6 Z^0$ events. No systematic errors are included in this plot.

If $M_t > M_{Z^0}/2$, we will have to rely on LEP II, LEP III and SLC II to find the top quark. This will constitute a search in the continuum similar to that described for TRISTAN earlier in this section.

4.2 SEARCHING FOR AND STUDYING THE Z^0 AND $W^\pm$

It is entirely possible that the Z^0 and/or $W^\pm$ will be discovered soon at CERN in the $\bar{p}p$ collider experiments. We still need to discuss the e^+e^- option because (a) CERN might not find them and (b) the copious, background free production in e^+e^- for the Z^0, in particular, will permit tests of the standard model far more thorough and precise than offered by the $\bar{p}p$ collider.

If the Z^0 is found at $M_{Z^0} = (93 \pm 2)$ GeV/c^2, this will be yet another triumph for the standard model. If a Z^0 is found either higher or lower (or both) than the

predicted value, then probably $SU(2) \wedge U(1)$ is not the correct group. This will be discussed in Sec. 7.1.

If the Z^0 is found at its standard model mass value, then even more stringent tests can be made of the standard model by running at and near the Z^0. A careful measurement of the Z^0 line shape will yield a precise measurement of M_{Z^0}. As noted in Sec. 3.3, this will permit a check on the radiative correction calculations for $sin^2\theta_W$. The measurement of M_{Z^0} from the Z^0 line shape is complicated by effects such as initial state radiation and beam dynamics and is by no means a simple task. However, if a precision of 300 MeV/c^2 can be obtained for M_{Z^0} this would correspond to an error of 0.0015 in $sin^2\theta_W$ (see Ref. 5a).

It will be possible at the SLC and LEP to measure all six leptonic coupling constants $v_e, a_e, v_\mu, a_\mu, v_\tau$, and a_τ and hence test $e/\mu/\tau$ universality. Since $v_f = sin^2\theta_W - \frac{1}{4}$ this will constitute another measurement of $sin^2\theta_W$. The quantities to be measured are

1. The charge asymmetry for each lepton f

$$A_{ch}^f = P_f \left[\frac{P(Z^0) + P_e}{1 + P_e P(Z^0)}\right](2cos\theta/1 + cos^2\theta)$$

where P_e is the polarization of the electron beam (the positrons are assumed to be unpolarized), $P_f = \frac{2v_f a_f}{v_f^2 + a_f^2}$ is the natural polarization of the fermion f coming from unpolarized Z^0's due to the fact that $g_L \neq g_R$, $P(Z^0) = 2v_e a_e/v_e^2 + a_e^2$ is the polarization of the Z^0 for unpolarized beams, and θ is the polar angle of the positively charged fermion.

2. The total rate

$$R_f = \frac{\sigma(f\bar{f})}{\sigma_{point}}$$

$$\propto (a_f^2 + v_f^2)(a_e^2 + v_e^2) \ .$$

If we integrate over the polar angle θ and assume that $p_e = 0$ we find

$$A_{ch}^f = \frac{3a_e\, v_e\, a_f\, v_f}{(a_e^2 + v_e^2)(a_f^2 + v_f^2)} \ .$$

Hence a measurement of A_{ch}^{e} and R_e will yield $|a_e|$ and $|v_e|$. If one measures the polarization of the τ (or μ in principle, but this is not practical) then from

$$\frac{A_{ch}^{\tau}}{P_\tau} = \frac{3}{2}\frac{a_e v_e}{(a_e^2 + v_e^2)}$$

one obtains also the relative sign of $|v_e|$ and $|a_e|$. Then from measurements of all R's and A_{ch}'s, the six coupling constants can be measured. The measurement of the charge asymmetry and lepton rates is not experimentally difficult and is routinely done[18] at PETRA and PEP. The measurement of P_τ has been studied extensively in the SLC workshop (see Ref. 5b, page 85). The spectrum of the π, e or μ in the decays $\tau \to \pi\nu_\tau$, $\tau \to e\nu_\tau \bar{\nu}_e$ and $\tau \to \mu\nu_\tau \bar{\nu}_\mu$ are modified by the polarization of the parent τ. In the case of $\tau \to \pi\nu_\tau$ the flat π energy spectrum obtained for an unpolarized τ becomes

$$\frac{dn}{dx_\pi} = 1 + P_\tau(2x_\pi - 1) \ ,$$

where $x_\pi = 2E_\pi/E_{c.m.}$, when the τ has polarization P_τ. Hence a measurement of the energy spectrum of the π yields a measurement of P_τ. The details of the experimental measurement are clearly given in Ref. 5b. Suffice it to say that with even a modest general purpose detector the measurement is readily made.

The presence of longitudinally polarized beam electrons makes things much easier. First of all we note that

$$A_{ch}^{f} = v_f v_e \sim v^2 \qquad \text{for } P_e = 0$$

$$\simeq v_f \qquad \text{for } P_e \approx 0.5$$

and, since the vector coupling constant is small (~ 0.02), polarized beams enhance markedly the observed charge asymmetry. Figure 11 shows the charge asymmetry as a function of $E_{c.m.}$ for the standard model with $sin^2\theta_W = 0.23$. Curves for unpolarized beams (0) and both orientations of longitudinally polarized electrons (R and L) are shown. In order to achieve a sizeable charge asymmetry with unpolarized beams requires moving off the resonance peak. This costs rate as shown by the dashed curve. However, with polarized beams the charge asymmetry is large on the resonance peak.

The use of polarized beams also alleviates the need for the τ polarization measurement. Consider the longitudinal spin flip asymmetry given by

$$A_L(\theta) = \frac{\frac{d\sigma}{d\Omega}(\theta, P_e = +) - \frac{d\sigma}{d\Omega}(\theta, P_e = -)}{\frac{d\sigma}{d\Omega}(\theta, P_e = +) + \frac{d\sigma}{d\Omega}(\theta, P_e = +)}$$

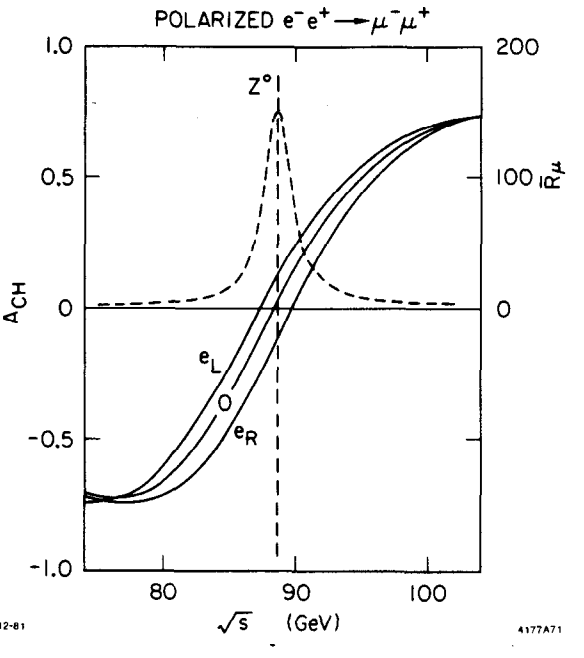

Fig. 11. The charge asymmetry as a function of $E_{c.m.}$ is shown for polarized and unpolarized beams according to the predictions of the standard model with $sin^2\theta_W = 0.23$. Also shown as a dashed curve is $R_\mu = \sigma(\mu^+\mu^-)/\sigma_{point}$.

Writing out this expression and integrating over any interval which is symmetric about $\theta = 90^o$ yields

$$A_L = P_e\left[\frac{2v_e a_e}{v_e^2 + a_e^2}\right]$$

one thus measures the relative sign of $|v_e|$ and $|a_e|$. At the Z^0 peak, A_L is large, measuring $\sim 16\%$ for $P_e = 0.5$ and $sin^2\theta_W = 0.23$.

The accuracy with which one obtains $sin^2\theta_W$ and the coupling constants is discussed in Ref. 5b, page 28. We summarize here by saying that for a sample of 10^6 Z^0 decays and a 3% branching ratio to $\mu^+\mu^-$ one obtains from the $\mu^+\mu^-$ channel

$$\left.\begin{aligned}\delta(sin^2\theta_W) &\simeq 0.002\\ \delta(v_\mu/a_\mu) &\simeq 0.008\end{aligned}\right\} \text{ from } A_{ch}$$

and

$$\left.\begin{aligned}\delta(sin^2\theta_W) &\simeq 0.001\\ \delta(v_\mu/a_\mu) &\simeq 0.008\end{aligned}\right\} \text{ from } A_L$$

It should be clear from the above discussion that measurements at the Z^0 will test the standard model very stringently. Any cracks in the armor will surely show up.

What about the $W^{\pm}$? Below W^+W^- threshold, we could look for the process shown in Fig. 12, namely $e^+e^- \rightarrow W^{\pm}e^{\mp}\nu_e$. However, the cross section for this process is $10^{-37} - 10^{-38}\ cm^2$ and for an average luminosity of $10^{31}\ cm^{-2}\ sec^{-1}$ and a cross section of $5 \times 10^{-38} cm^2$ the rate for this process would be 5×10^{-2} events/day. Given that these events would have to be extracted from a hadronic background of $\sim$ 10 events/day, this avenue does not look promising. So we investigate the process $e^+e^- \rightarrow W^+W^-$ which proceeds via the three graphs shown in Fig. 13 with a production cross section as shown in Fig. 14. There is some usable production cross section at 170 GeV which is chosen since it is the highest LEP II energy. At this energy $\sigma_{W^+W^-} \simeq 7 \times 10^{-36}\ cm^{-2}$ and for $< L >= 5 \times 10^{31}\ cm^{-2}\ sec^{-1}$ one would obtain 20 W^+W^- events/day. A topology which would be readily observable would be

$$\begin{array}{l} e^+e^- \rightarrow W^+ \quad W^- \\ \qquad\quad\ \ \big| \qquad\ \big| \rightarrow q\bar{q} \\ \qquad\quad\ \ \big| \\ \qquad\quad\ \ \big| \rightarrow \ell^+\nu_e \end{array} \tag{3}$$

where ℓ refers to a charged lepton. The events would have a single lepton in one hemisphere and a hadron jet in the other. Further confirmation of the process (3) would come from the measurement of the hadron jet mass which would reconstruct to the $W^{\pm}$ mass. The W coupling strength to fermions is democratic and hence for $N = 3$ generations

$$\frac{\Gamma(W \rightarrow \ell\nu)}{\Gamma(W \rightarrow ALL)} = \frac{1}{4N} = \frac{1}{12}$$

$$\frac{\Gamma(W \rightarrow q\bar{q})}{\Gamma(W \rightarrow ALL)} = \frac{3}{4N} = \frac{1}{4} \ .$$

Summing over the possible quark final states and assuming either the $e\nu_e$ or $u\nu_\mu$ possibility of the leptonic decay, the topology of (3) would yield 5 W^+W^- events/day. This signal should not be missed.

The measurement of $\sigma(e^+e^- \rightarrow W^+W^-)$ is an important test of the gauge structure of $SU(2) \wedge U(1)$. If $g_{Z^0W^+W^-}$ were zero, some of the cancellations occurring in the contributions from interference terms (see Fig. 13) would vanish, and $\sigma(e^+e^- \rightarrow W^+W^-)$ would roughly double. In this way e^+e^- interactions would offer a unique test of the standard model unavailable at the $\bar{p}p$ collider.

Fig. 12. $e^+e^- \rightarrow W^\pm e^\mp \nu_e$.

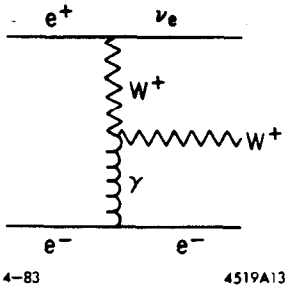

Fig. 13. The three processes which contribute to $e^+e^- \rightarrow W^+W^-$.

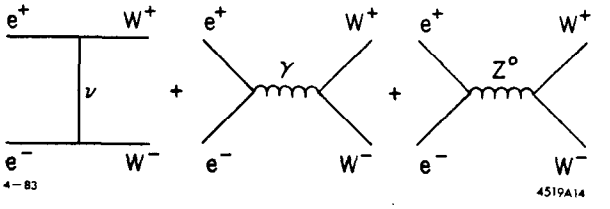

Fig. 14. The cross section for $e^+e^- \rightarrow W^+W^-$ as calculated in the standard model. The maximum LEP II energy is shown.

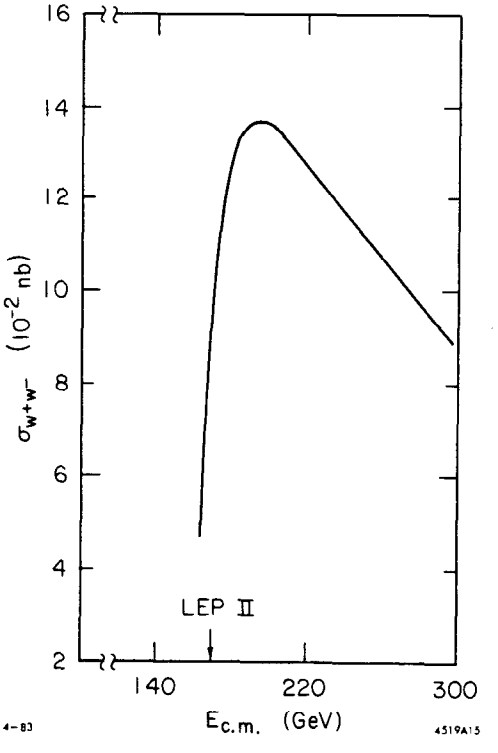

4.3 SEARCHING FOR THE NEUTRAL HIGGS PARTICLE, H^0

The Higgs mechanism is probably the most controversial part of the standard model because it requires very precise fine tuning to work. (See the lectures of Susskind, these proceedings.) Because the mass of the H^0 is not predicted by the theory it is also one of the most difficult areas of the theory to test. The two most promising places to search for the H^0 in e^+e^- interactions is at toponium and the Z^0.

Consider the decay of a heavy $Q\bar{Q}(1^{--})$ state, V, into $H^0\gamma$ as shown in Fig. 15a. This process was first discussed by Wilczek.[19] For $M_{H^0} \ll M_V$, the decay rate for this process is given by

$$\frac{\Gamma(V \to H^0\gamma)}{\Gamma(V \to e^+e^-)} \simeq \frac{\mathcal{G}_F M_V^2}{4\sqrt{2}\,\pi\alpha}\left[1 - \frac{M_{H^0}^2}{M_V^2}\right] .$$

Considering then the two upcoming toponium sources, we find

	$E_{c.m.}$ GeV	$< \mathcal{L} >$ $cm^{-2}sec^{-1}$	# V per day	$\frac{\Gamma(V\to H^0\gamma)}{\Gamma(V\to ee)}$	$\Gamma(V \to ee)$ %	# $V \to H^0\gamma$ per day
PETRA	40	1.6×10^{31}	400	0.14	6	3.4
TRISTAN	60	2×10^{31}	220	0.32	6	4.2

where we have used the estimates[20] in Fig. 16 to obtain the rates above. The production rate for toponium $\to H^0\gamma$ at both PETRA and TRISTAN is quite favorable. What about the event shapes? The photon in the decay of toponium $\to H^0\gamma$ will be monochromatic with its energy given by

$$X_\gamma^{H^0} = 2E_\gamma/E_{c.m.} = \left(1 - \frac{M_{H^0}^2}{M_V^2}\right) .$$

The decay of the H^0 will be predominantly to the heaviest fermion pair available and estimates for H^0 branching fractions as a function of M_{H^0} are given in Fig. 17. The event shape will depend on M_{H^0} but in essence the events will have a monochromatic photon in one hemisphere and a hadron jet in the other hemisphere (see Fig. 15b). The main background will come from the process shown in Fig. 15c, $V \to gg\gamma$, where the symbol g is used to denote a gluon. From Fig. 16 we see that

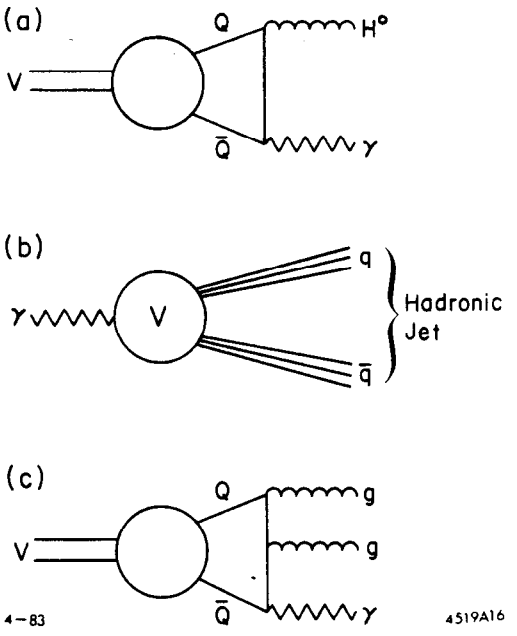

Fig. 15. The decay of heavy quarkonium $V \rightarrow H^0\gamma$ is shown in (a). In (b) H^0 decays to a quark antiquark pair and (c) shows the main background for (a) namely $V \rightarrow gg\gamma$.

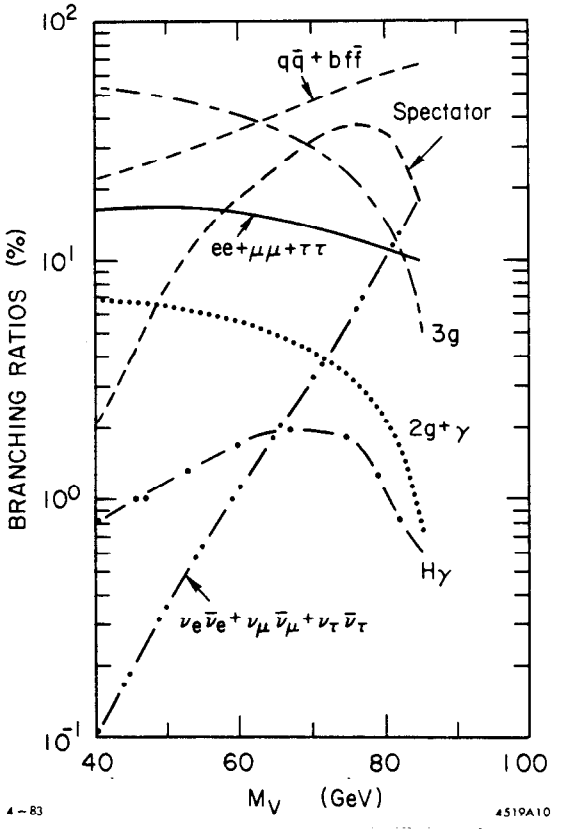

Fig. 16. The quarkonium branching fractions are shown (taken from Ref. 20) as a function of the quarkonium mass. The neutral Higgs boson mass was taken to be 10 GeV/c^2.

$$\frac{\Gamma(V \to gg\gamma)}{\Gamma(V \to H^0\gamma)} \simeq 7 \quad \text{at} \quad M_V = 40\ \text{GeV/c}^2$$

$$\simeq 3 \quad \text{at} \quad M_V = 60\ \text{GeV/c}^2 \ .$$

This background is distinguishable from the signal when we use the property that the photon from the signal is monochromatic. Roughly speaking the photon spectrum from the background in linear

$$\frac{dn}{dX_\gamma} \simeq X_\gamma \qquad \text{for} \quad V \to gg\gamma \ .$$

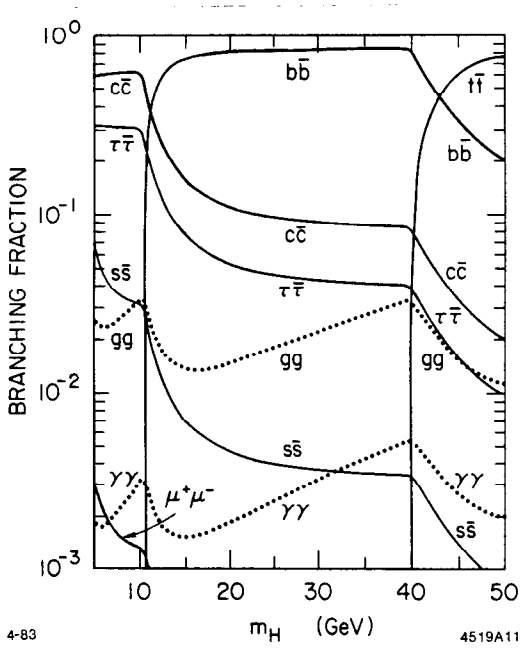

Fig. 17. Decay modes of the neutral Higgs boson as a function of its mass.

Assume that the photon is measured in a calorimeter whose energy resolution $\sigma_E/E = \sigma_X/X = .1/\sqrt{E}$. For $X_\gamma > 0.5$ $\sigma_{X_\gamma} \simeq 2\%$ As an example consider that $M_V = M_{t\bar{t}} = 60\ \text{GeV/c}^2$ then for

$$M_{H^0} = 20\,\text{GeV}, \quad X_\gamma^{H^0} = 0.89 \quad \text{or} \quad E_\gamma = 27\,\text{GeV}$$
$$= 10\,\text{GeV}, \quad X_\gamma^{H^0} = 0.97 \quad \text{or} \quad E_\gamma = 29\,\text{GeV} \ .$$

Figure 18 depicts the experimental problem, namely with a resolving width of 2% and $X_\gamma = 0.89$, can we sort out the signal from a background which is three times as copious? The figure is drawn so that the relative areas of the Gaussian (signal) and

the triangle (background) are 1 : 3 and the Gaussian has a width of 2% . One sees that indeed the signal would readily be seen. With enough data one could remove the background by requiring the $H^0 \to \tau^+\tau^-$ decay. For $M_{H^0} = 10$ GeV/c^2, $B(H^0 \to \tau^+\tau^-) = 30\%$ and one pays an acceptable price. For $M_{H^0} = 20$ GeV/c^2, $B(H^0 \to \tau^+\tau^-) = 5\%$ and a long run would be needed to establish the H^0 if one required the $H^0 \to \tau^+\tau^-$ decay mode.

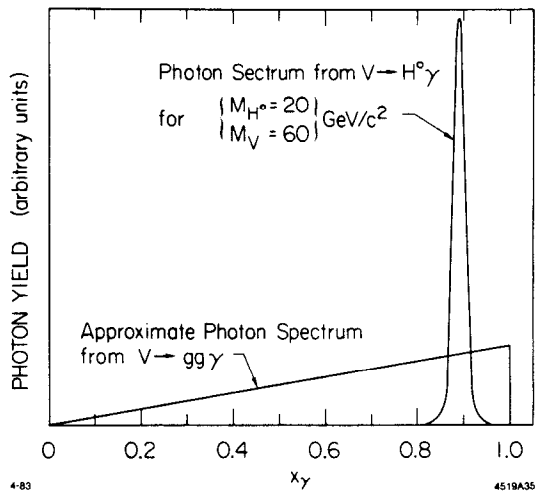

Fig. 18. The photon spectrum from $V \to H^0\gamma$ assuming $M_{H^0} = 20$ GeV/c^2, $M_V = 60$ GeV/c^2 and $\sigma_E/E = 10\% / \sqrt{E}$. Also shown in an approximation to the photon spectrum for the background $V \to gg\gamma$. The relative areas of the two curves are chosen to simulate the expectations for these two processes.

Having established the signal, how well could one measure M_{H^0}? One could either measure the jet mass or obtain the mass from the measured photon energy. It is hard to estimate how well one would do using the former method because it will depend on the characteristics of the detector and on Monte Carlo corrections. For the latter method

$$X_\gamma = \left(1 - \frac{M_{H^0}^2}{M_V^2}\right) \Rightarrow \sigma_{M_{H^0}} = \frac{M_V^2}{2M_{H^0}} \sigma_{X_\gamma} \ .$$

For $\sigma_E/E = .1/\sqrt{E}$ and $M_{H^0} = 20$ GeV/c^2 and $M_V = 60$ GeV/c^2 one finds $\sigma_{M_{H^0}} = 1.8$ GeV/c^2.

We can conclude that for $M_{H^0} \leq M_{t\bar{t}}/2$, toponium should yield the H^0 via the decay toponium $\to H^0\gamma$. Suppose that either $M_{H^0} > M_{t\bar{t}}/2$ or the SLC turns on at about the same time as TRISTAN. Can one search for the H^0 at the Z^0? Bjorken[21] pointed out that indeed one could utilize the process $Z^0 \to$ virtual $Z^0 + H^0 \to H^0\ell^+\ell^-$ as shown in Fig. 19. Here $\ell^\pm$ are charged leptons. The production rate[22] for this process is shown in Fig. 20. Also shown is the rate for $Z^0 \to H^0\gamma$ which vanishes in

first order because the photon and the Z^0 are "orthogonal." The $Z^0 \rightarrow H^0\ell^+\ell^-$ event rate is not large and will require that the SLC and LEP obtain their promised peak luminosity.

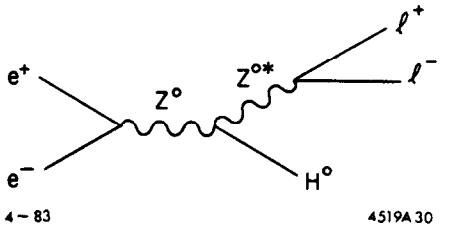

Fig. 19. The process $e^+e^- \rightarrow Z^0 \rightarrow H^0\ell^+\ell^-$.

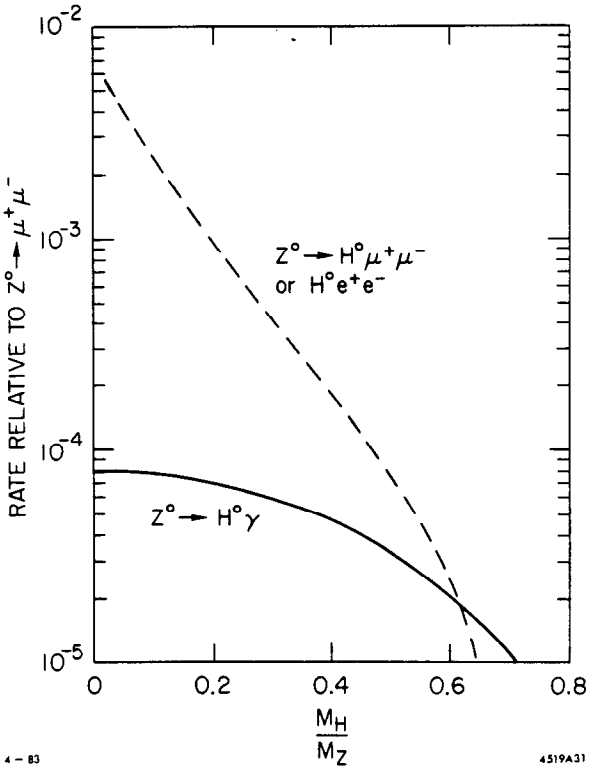

Fig. 20. The decay rate for $Z^0 \rightarrow H^0e^+e^-$ or $Z^0 \rightarrow H^0\mu^+\mu^-$ relative to $Z^0 \rightarrow \mu^+\mu^-$ which has a branching fraction of 3% .

For a $< \mathcal{L} >= 3 \times 10^{30}\ cm^{-2}\ sec^{-1}$ the event rates for each lepton channel are 1.2/day for $M_{H^0} = 10$ GeV/c^2, 0.4 events/day for $M_{H^0} = 20$ GeV/c^2 and 0.3 events/day for $M_{H^0} = 30$ GeV/c^2. This signal must be observed in the presence of a hadronic event rate of ~9,000 events/day. The key to extracting a signal is the event topology. The dilepton pair take most of the energy in the process, leaving the H^0 close to rest. Figure 21 shows the dilepton invariant mass spectrum for different values

of M_{H^0}. The slow H^0 is assumed here to decay to a pair of quarks. What results then is an event with two quark jets which are roughly back to back and a pair of high energy leptons whose direction is not correlated to the hadronic sphericity axis. Figure 22 shows this topology schematically. There have been numerous studies of the detection of these $H^0\ell^+\ell^-$ events at the various Z^0 workshops; we have used the study done for the SLC workshop.[5b] Hadronic events at the Z^0 were produced using a Monte Carlo simulation program. Events were selected which had two electrons (muons will look essentially the same). Figure 23 shows the dilepton mass spectra which arise from the signal and the $Z^0 \rightarrow$ *hadrons* background. In order to reduce the background, each lepton is required to have an angle $>$ 200 mrad relative to the sphericity axis of the hadronic system. This will cause virtually no loss ($\sim 2 \times 200/2 \times \pi \times 10^3 =$ 6%) of signal events because the leptons have no correlation to the hadronic system. However, the background is substantially reduced because the main source is $Z^0 \rightarrow t\bar{t}$ where both t's decay semileptonically and in this case it is rare to get two high energy decay leptons which have, in addition, large transverse momentum. It appears then as if the hadronic background can be handled.

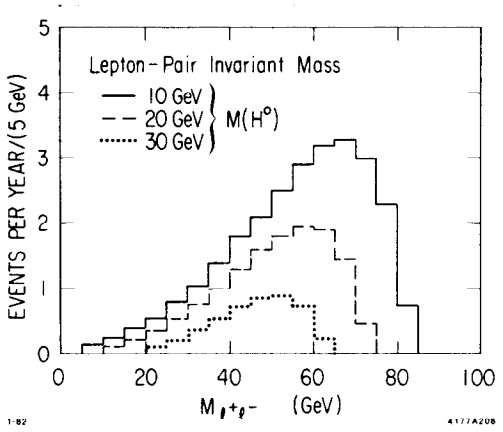

Fig. 21. Dilepton mass spectra for $Z^0 \rightarrow H^0\ell^+\ell^-$ for several choices of the Higgs mass. The normalization corresponds to 2000 hours of beam time at an average luminosity of $10^{30}\ cm^{-2}\ sec^{-1}$.

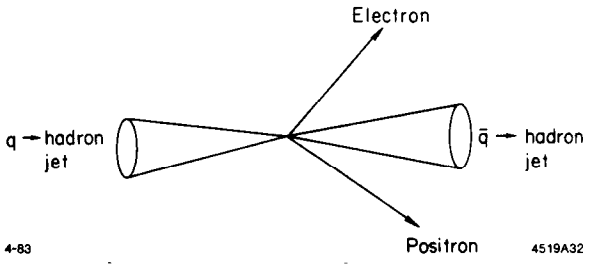

Fig. 22. A schematic representation of the topology of the $Z^0 \rightarrow H^0e^+e^-$ events.

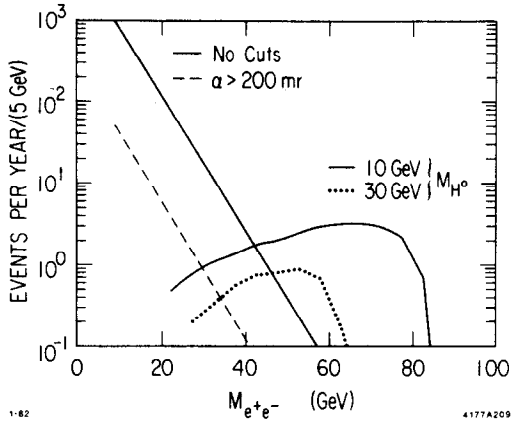

Fig. 23. The electron-positron pair mass spectra for: (a) e^+e^- pairs from jets without cuts (solid line), (b) e^+e^- pasirs from jets with a 200 mrad cut described in text (dashed line), and (c) e^+e^- pairs from $Z^0 \rightarrow H^0e^+e^-$, $M_{H^0} = 10$ GeV/c^2 (solid line) and $M_H = 20$ GeV/c^2 (dashed line).

In order to establish a signal, one must look for a peak in the spectrum of the mass recoiling against the dilepton pair. This recoil mass is shown in Fig. 24 for $M_{H^0} = 10$ GeV/c^2 assuming that one detects electrons in an electromagnetic calorimeter with an energy resolution of $\sigma_E/E = 10\% / \sqrt{E}$. A clear signal is seen with a mass resolution of roughly 1 GeV/c^2. The mass resolution degrades approximately linearly with the calorimeter resolution and, particularly for a high mass H^0, one would not want to do this measurement with a calorimeter having an energy resolution worse than $20\% / \sqrt{E}$. If the muon channel is chosen the muon momentum resolution required which corresponds to $\sigma_E/E = 20\% / \sqrt{E}$ is $\sigma_{P/P} = 0.1\% P$ assuming that the typical lepton momentum is 30 GeV/c. Because the rate is so small an optimal detector should have good solid angle coverage and be able to detect both the dielectron and dimuon modes. The requirements for lepton/hadron separation are not too taxing; a rejection of 50 : 1 would be more than adequate.

We can summarize this discussion by saying that searches for the H^0 will be possible at the SLC and LEP provided that these machines achieve their design luminosities of $\geq 5 \times 10^{30}\ cm^{-2}\ sec^{-1}$. Experiments will have sensitivity to the mass range $5 \leq M_{H^0} \leq 40$ GeV/c^2. The upper limit comes from rate and hadronic background limitations and the lower limit from backgrounds arising from two photon processes which were not discussed here (see Ref. 5b).

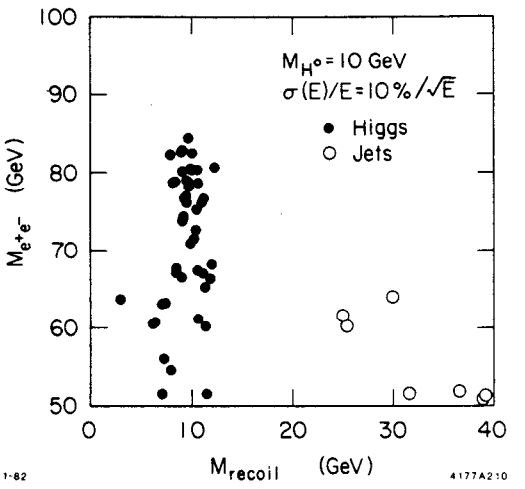

Fig. 24. Scatter plot of $M(e^+e^-)$ versus recoil mass where a calorimeter with resolution $\sigma_E/E = 10\% \, / \sqrt{E}$ is assumed.

Assume nature is unrelenting and $M_{H^0} > 40$ GeV. Searches will have to be performed at LEP II, LEP III and SLC II and possibly at the high energy colliding linacs. The H^0 can be pursued using the reaction $e^+e^- \rightarrow H^0Z^0$ where the dominant contribution to the process comes from an intermediate virtual Z^0 as shown in Fig. 25. The cross section for this process is given by[23]

$$\sigma(e^+e^- \rightarrow Z^0H^0) = \frac{\mathcal{G}_F^2 M_{Z^0}^2}{48\pi} f(s, M_{Z^0}, M_{H^0})(1 - 4sin^2\theta_W + 8sin^4\theta_W)$$

where $\sqrt{s} = E_{c.m.}$ and

$$f(s, M_{Z^0}, M_{H^0}) = \frac{1}{s}[1-A]^{\frac{1}{2}}[1-B]^{\frac{1}{2}}\left\{(1-A)(1-B) + 12\frac{M_{Z^0}^2}{s}\right\}\left[\frac{1}{(1-\frac{M_{Z^0}^2}{s})^2}\right]$$

and $A = (M_{Z^0} + M_{H^0})^2/s$, $B = (M_{H^0} - M_{Z^0})^2/s$. Figure 26 shows the ratio of $\sigma(e^+e^- \rightarrow Z^0H^0)$ to the point cross section as a function of $E_{c.m.}$ and M_{H^0}. The cross section for $e^+e^- \rightarrow Z^0H^0$ is comparable to the point cross section and therefore the event rates will be favorable. For fixed $E_{c.m.}$ the cross section remains independent of M_{H^0} until one comes close to threshold. As $E_{c.m.}$ is increased, the relative rate decreases quite rapidly.

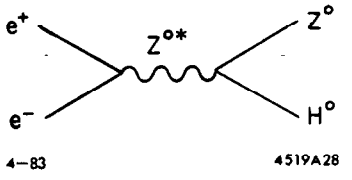

Fig. 25. The process $e^+e^- \rightarrow Z^{0*} \rightarrow Z^0H^0$.

Running at the highest LEP II energy of $E_{c.m.} = 170$ GeV the event rate for a H^0 with a mass of 40 GeV/c^2 is ~ 3 events/day. This assumes a $< \mathcal{L} >= 1.6 \times 10^{31}\ cm^{-2}\ sec^{-1}$. The final state Z^0H^0 must be extracted from a hadronic background of ~ 15 events/day. In general these two processes will not easily be separated. One could guarantee separation by requiring that the $Z^0 \rightarrow e^+e^-$ or $\mu^+\mu^-$ or $\tau^+\tau^-$ or $\nu\bar{\nu}$. This constitutes 3% of the Z^0 decays per charged lepton pair plus 9% for the $\nu\bar{\nu}$ channel. In the lepton decay channels one would have an extra handle on the process by calculating the dilepton invariant mass which should be the Z^0 mass. The H^0 mass would have to be reconstructed from the H^0 decay products.

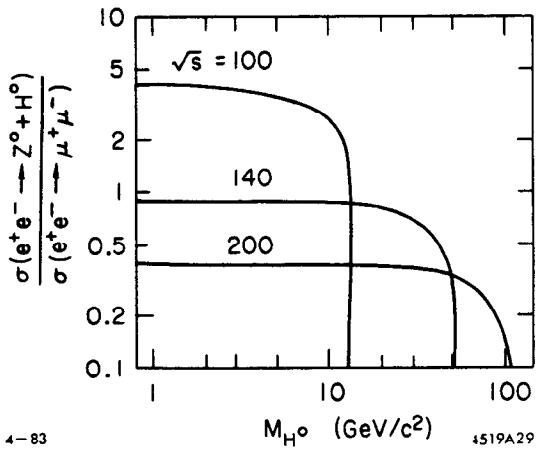

Fig. 26. The rate[23] for the process $e^+e^- \rightarrow Z^0H^0$ is shown as a function of $E_{c.m.}$ and M_{H^0}. The rate is normalized to the point cross section which has the value $86.8/E^2_{c.m.}$ nb.

The search for the H^0 at LEP II and LEP III will be possible for H^0 masses $\leq \frac{E_{c.m.}}{2}$ provided that these machines achieve their design luminosity. For very heavy H^0's, those which would be found at the colliding linacs, a luminosity of $10^{32} - 10^{33}\ cm^{-2}\ sec^{-1}$ is needed.

4.4 Tests of the Non-Abelian Nature of QCD

We first consider the evidence which exists for gluons. Such evidence comes from e^+e^- interactions at PETRA, PEP and CESR and from deep inelastic lepton scattering. For an excellent review of this topic see Ref. 24. In all respects the data are in good agreement with the predictions of QCD and no conflicts exist. In particular, QCD predicts the presence of three jet events in e^+e^- at $E_{c.m.} \geq 10$ GeV and indeed such events are seen. Let us review the evidence for the three jet events as obtained by the PETRA groups and confirmed recently by the PEP experiments.

The first striking property of the hadronic events at PETRA is that the mean transverse momentum of particles relative to the thrust or sphericity axis grows with increasing $E_{c.m.}$. The growth of the average p_T occurs in the plane containing most of the momentum, the $< p_T >$ out of this plane is almost independent of $E_{c.m.}$. These effects are shown in Fig. 27. If one looks at the high energy hadronic events clear three jet structures are seen. A model using only the process $e^+e^- \rightarrow q\bar{q}$, in which the quark mean p_T in the fragmentation process is allowed to grow with $E_{c.m.}$, does not account for the growth of $< p_T >$ in the event plane. The interpretation of the data is that the growth of $< p_T >$ in the plane occurs because of the emission of

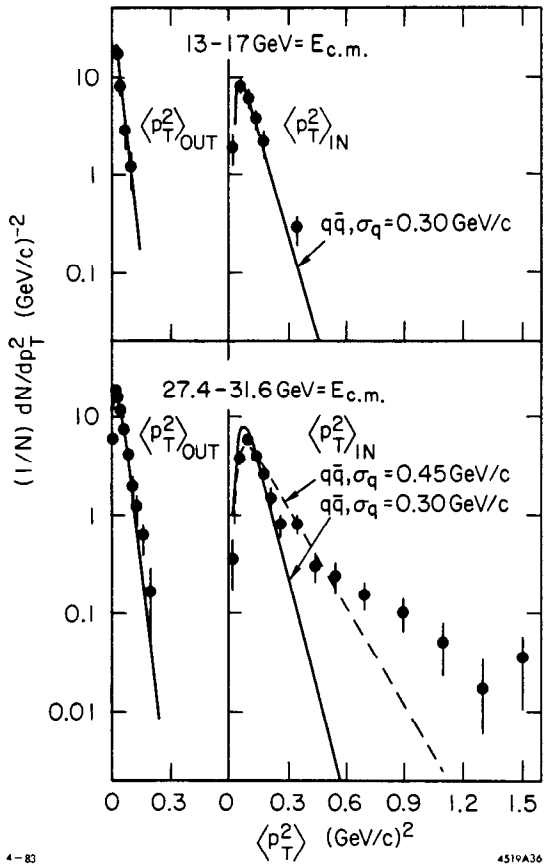

Fig. 27. The mean transverse momentum squared per event is shown both normal to the event plane ($< p_T^2 >_{out}$) and in the event plane ($< p_T^2 >_{in}$) at $E_{c.m.} = 13$, 17 and 27.4 - 31.6 GeV. These data are from the TASSO group. The predictions of the quark model ($e^+e^- \rightarrow q\bar{q}$) are shown assuming the quark fragmentation process is characterized by a $\sigma_q = 300$ MeV/c (solid line) or $= 450$ MeV/c^2 (dashed line).

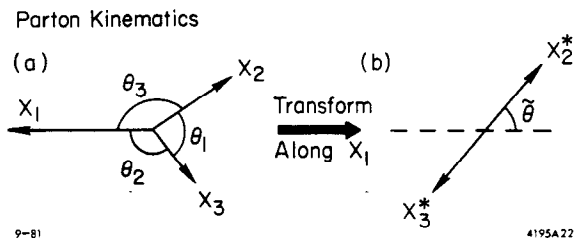

Fig. 28. (a) The kinematics for the process $e^+e^- \rightarrow qqg$ where $x_i = E_i/E_{c.m.}$ and E_i are the parton energies. (b) The definition of the Ellis-Karliner angle, $\tilde{\theta}$.

a gluon(s) namely $e^+e^- \rightarrow qqg$. This process can be thought of as bremsstrahlung of a gluon off a quark (antiquark) line. The process is shown pictorially in Fig. 28a. QCD predicts, to first order in α_s, the distribution of the parton momenta

$$\frac{1}{\sigma_0}\frac{d\sigma}{dx_1 dx_2} = \frac{2\alpha_s}{3\pi}\left[\frac{x_1^2+x_2^2}{(1-x_1)(1-x_2)} + \begin{matrix}(1,2,3)\\ cyclic\ \ permutations\end{matrix}\right]$$

where $X_i = 2E_i/E_{c.m.}$ and E_i is the parton energy. The analyses performed at PETRA constitute tests of the above Dalitz plot distributions ($\Sigma x_i = 2$). For example the measured distribution of x_1 in clear three jet events is shown in Fig. 29 along with the prediction of the QCD Monte Carlo. These tests have been performed by all the PETRA groups[25] and the MARK II at PEP[26] and in all cases the data are well represented by the QCD Monte Carlo simulation programs. We omit here the discussion of how the three jet events are obtained. There are many methods for doing this[27] and suffice it to say that for the conclusions above all these methods are reasonable. As another check on these Dalitz plot distributions, the spin of the assumed gluon has been measured. The method employed by the TASSO and MARK II group is that suggested by Ellis and Karliner[28] in which one transforms to the rest frame of the (x_2, x_3) system using the measured direction and velocity of the fastest parton (x_1). This is shown pictorially in Fig. 28b. $\tilde{\theta}$ is the decay angle in this (x_2, x_3) rest frame and $dN/(d\cos\tilde{\theta})$ can be thought of as the decay angular distribution of the gluon which will be sensitive to the spin of the gluon. If one assumes that the partons are massless

$$\cos\tilde{\theta} = \frac{x_2 - x_3}{x_1} .$$

Figure 30 shows the $\cos\tilde{\theta}$ distribution for clear three jet events as obtained by TASSO.[25] The prediction of QCD for spin 1 and spin 0 gluons is also shown. The spin 1 hypothesis reproduces the data well, the spin 0 hypothesis is a poor representation of the data. To quantify this, TASSO finds

$$< \cos\tilde{\theta} >_{data} = 0.3391 \pm 0.0079$$

$$< \cos\tilde{\theta} >_{data} - < \cos\tilde{\theta} >_{QCD} = 0.0019 \pm 0.0084 \quad \text{and}$$

$$< \cos\tilde{\theta} >_{data} - < \cos\tilde{\theta} >_{scalar\ gluon} = 0.0411 \pm 0.0084$$

Fig. 29. The parton thrust distribution as measured by the TASSO group. The solid curve is the prediction of QCD to leading order in α_s which is taken to be 0.17.

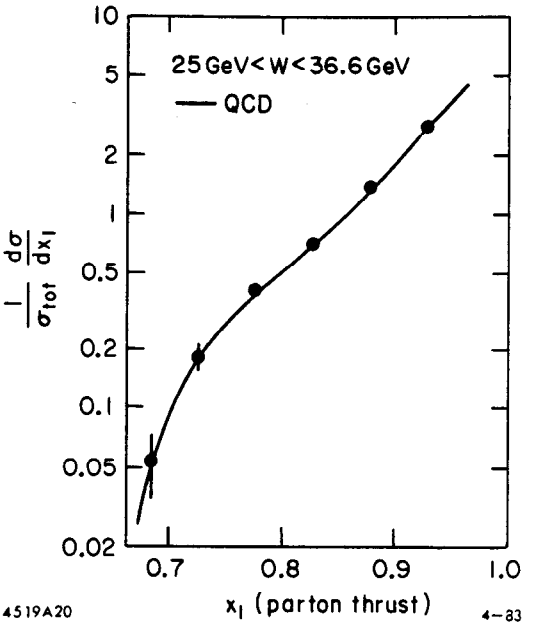

Fig. 30. The distribution of the Ellis-Karliner angle, $\tilde{\theta}$, for the three jet events with $x_1 < 0.9$ obtained by the TASSO group. The solid curve is QCD with $\alpha_s = 0.17$, the dashed curve is the prediction for a scalar gluon.

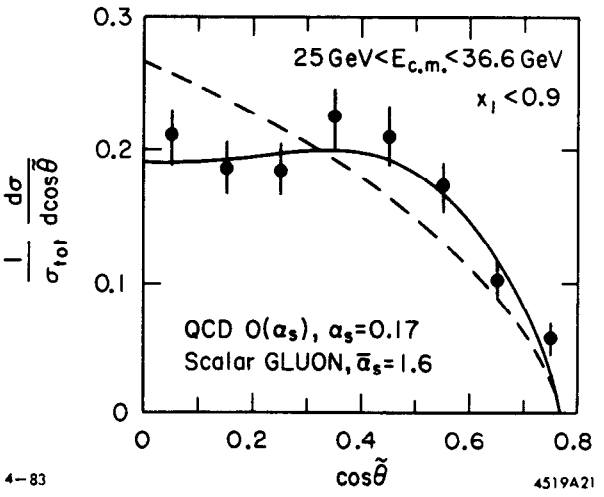

and hence the scalar gluon is ruled out at the five standard deviation level. This result is confirmed by the MARK II[29] and all the other PETRA groups.[25]

The groups running on the Υ first at DORIS[30] and more recently at CESR[31] have shown that the event shapes of the hadronic events agree very well with the QCD prediction that the Υ decays to three gluons. As an example, the data of the PLUTO group for thrust is shown in Fig. 31.

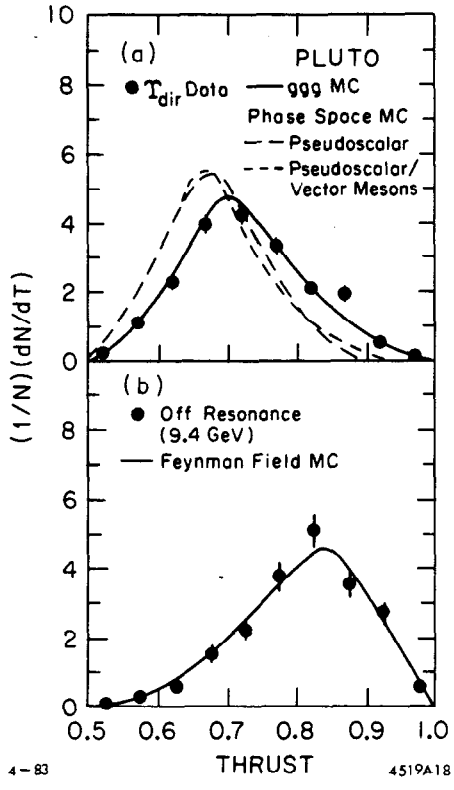

Fig. 31. The thrust distributions as measured by PLUTO for Υ and the continuum.

We can summarize by saying that in all these studies, the predictions of the first order QCD, as they are incorporated in Monte Carlo simulation programs, do an excellent job of accounting for the experimental data. QCD makes predictions for parton distributions and the experiments observe hadrons. The gap is bridged by models for this fragmentation process. The simulation programs have many adjustable parameters which give the experimenters some freedom when the comparisons are made. Hence some of the arguments become circular.

In the light of this criticism we should ask whether there are competing theories or models which can account for the observed data. We know that at energies $\leq$ 10 GeV, $e^+e^- \rightarrow q\bar{q}$ plus fragmentation of the quarks into hadrons account very well for the e^+e^- data. Can one make simple extensions to such models to account for the 30 GeV e^+e^- data? There are a wide variety of these extended $q\bar{q}$ models and in general one is able to arrange the parameters of the models to reproduce the $< p_T >$ distributions both in and out of the event plane. However in doing so the x_1 distributions never agree with the data. We borrow Table 5 directly from Ref. 25 to show the kinds of

models which have been tried. The notation $q_\perp$ is the quark transverse momentum, σ_q is the average of this quantity and x_1 is as discussed earlier in this section. Figure 32 indicates how the first and third models in Table 5 fail to account for the data. The other models fail in a similar way.

There is a model which is not a simple extension of $e^+e^- \rightarrow q\bar{q}$ whose proponents claim accounts well for the PETRA data. The model which goes under the name of Quantum Geometrodynamics (QGD), is due to G. Preparata and coworkers at Bari. The model has the somewhat uncomfortable feature of evolving with the evolving data and so a clear and complete reference is hard to find. However, the interested reader can start with the references given in Ref. 32.

Table 5. Comparison with Two Jet Models.

Model	Result	
$\frac{d\sigma}{dq_\perp^2} \sim exp\left(\frac{-q_\perp^2}{2\sigma_q^2}\right)$	$p_\perp^2$, $< p_\perp^2 >_{in}$, $< p_\perp^2 >_{out}$	good
$\sigma_q = 320$ GeV/c for u,d,s,	x_1	too low
$\sigma_q = 800$ MeV/c for c, b	$p_\perp^2$ w.r.t. 3 axes	too broad
$\frac{d\sigma}{dq_\perp^2} \sim exp\left(\frac{-q_\perp}{a}\right)$	$p_\perp^2$, $< p_\perp^2 >_{in}$, $< p_\perp^2 >_{out}$	good
	x_1	too low
$\frac{d\sigma}{dq_\perp^2} \sim exp\left(\frac{-dq_\perp^2}{2\sigma_q^2}\right) +$	$p_\perp^2$, $< p_\perp^2 >_{in}$, $< p_\perp^2 >_{out}$	good
$a\ q_\perp^{-4}$	x_1	too low

QGD differs greatly in motivation for QCD and in its Monte Carlo formulation it has far less parameters than QCD plus fragmentation. In particular the model does not have gluons and hence, while it predicts three jet events, it also predicts that the three jets should all fragment identically. This being a leading issue, we proceed to look at this model. The model is not easy to describe but we do our best in this limited space. At the heart of the model is an object called a "fire sausage" or "fire string" which is a bag in space-time. The concept is that one starts off with geometry – simple domains in space-time which contain a $q\bar{q}$ pair – and then, using a wave

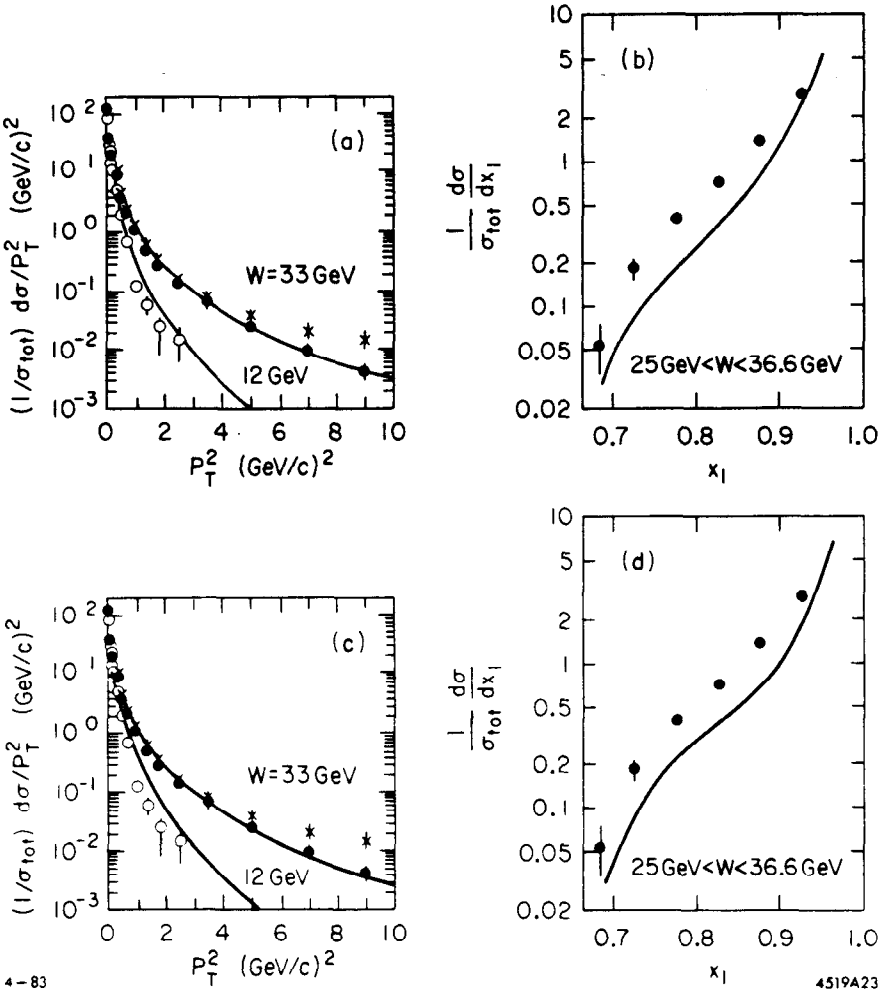

Fig. 32. The (TASSO) data in (a) and (c) are the same, namely the distribution of transverse hadron momentum squared with respect to the sphericity axis. For the high energy data, the parton thrust distribution is shown in (b) and (d). The fits to (a) and (b) are for the model described in column one of Table 5, and those to (c) and (d) are for the model described in column three of Table 5.

function for this domain and a set of physical boundary conditions, one generates dynamics. The dynamics comprise a particle spectrum and perturbative bag interactions. The particle spectrum which evolves is a set of Regge trajectories.

Multiparticle states originate from the decay of well defined $q\bar{q}$ structures — the fire strings (FS). These FS's are tube-like structures — see Fig. 33 — which contain a coherent superposition of Regge trajectories of different orbital angular momentum. In

three space you can visualize this object as containing $q\bar{q}$ waves moving freely inside a cylinder of length $R_\ell \sim mass$ and a radius $R_\perp \sim log(mass)$. There are two ways that the FS can decay and in both cases the process is specified by QGD without freedom of parameters. The two decay mechanisms, chain (a) and tree (b), are shown in Fig. 34. The kernels for these decays are predicted by QGD and the only parameter in the model is α which is the relative amount of chain and tree decay required by nature.

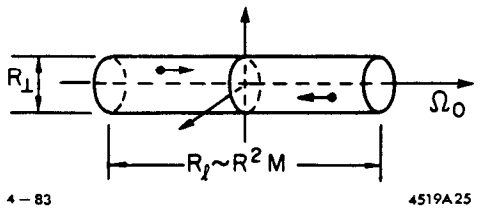

Fig. 33. A schematic representation of a fire-string (FS).

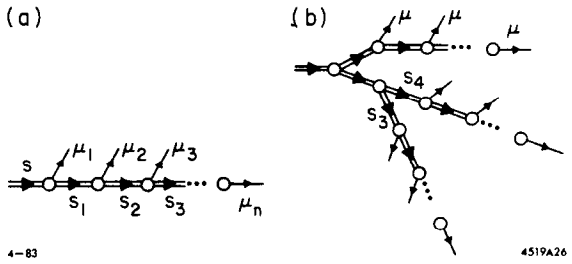

Fig. 34. The chain (a) decay and the tree (b) decay of a fire-string.

From this brief discussion it probably hasn't been clear, but the decay process outlined above is akin to hadronization plus perturbative QCD. In QGD, a FS is produced in e^+e^- with the quark content specified by the quark charge squared. The angular distribution of the axis of the FS is taken to be $1+cos^2\theta$ in the usual manner. A Monte Carlo simulation program, called EPOS, has been written incorporating the ideas outlined above. It has only one parameter α (or two if one adds in baryons as decay products of the FS). Using the TASSO data from PETRA, Preparata et al.,[32] have fit α and find it to be $\alpha = 1.05 \pm 0.3$. Having fixed this parameter, they then compare their Monte Carlo predictions with QCD and data. Figure 35 shows the comparison between QCD and QGD for the three jet kimenatics. At the parton level the agreement is good. Figure 36 shows the comparison between QGD and the TASSO hadron inclusive spectra. QGD agrees well with the data and even predicts the correct amount of scaling violations. More comparisons are given in the references. The reason for including this model was that in the eyes of its proponents a model, quite different than QCD, does account for the observed data and hence offers an alternative to the

notion of gluons. The model is, in principle, distinguishable from QCD in that it predicts that all jets should fragment identically, whereas QCD predicts that gluons should fragment differently than quarks. QGD offers an interesting straw man and it would be nice if the experimental groups could make direct comparisons between EPOS and their data.

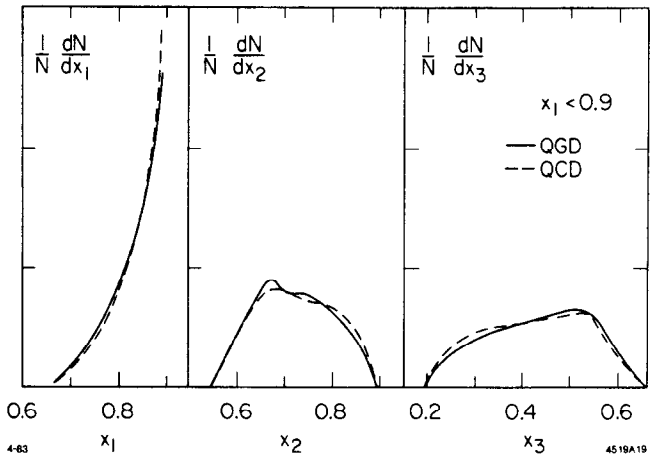

Fig. 35. A comparison between the three jet parton x distributions (see Fig. 28) for QCD and QGD.

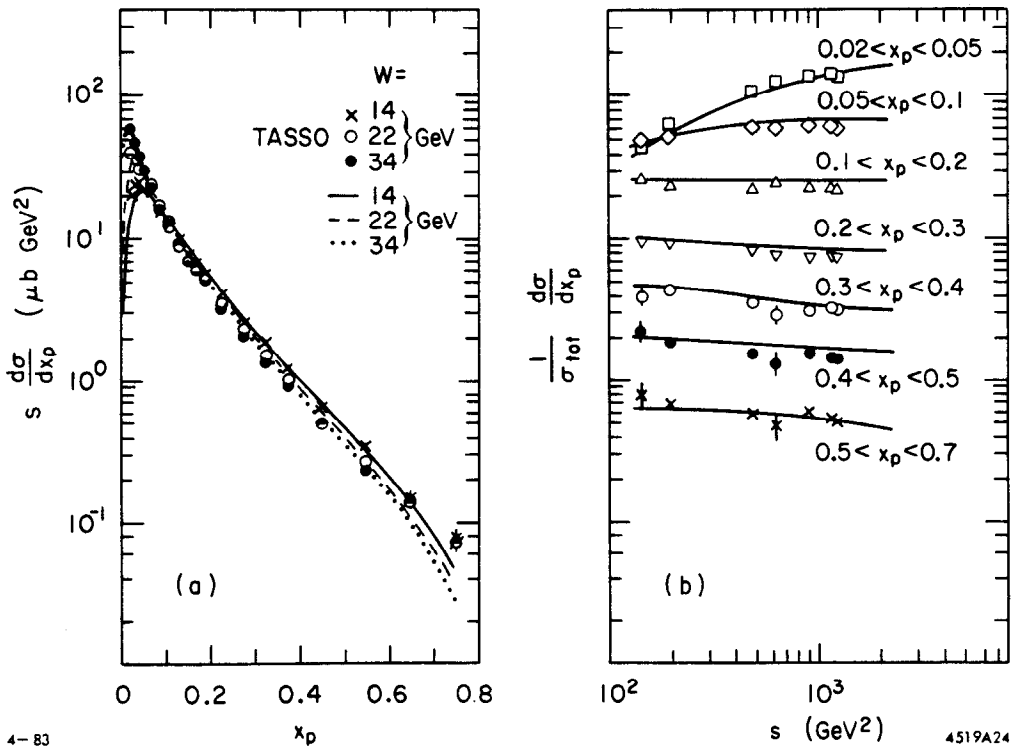

Fig. 36. Predictions of the QGD Monte Carlo simulation program EPOS are compared with the hadron inclusive spectra of TASSO (a) and with the scaling violations implied by the data (b).

The verification of first order QCD as discussed earlier in this section is most impressive. It is also nontrivial; we have seen only one (of many) alternative model achieve any measure of success. However to some extent the evidence in favor of QCD is circumstantial and we should have higher standards if we are to say that QCD is the "theory of the strong world." In particular we should demand more direct evidence that QCD is a non-Abelian theory.

The most natural place to look for the proof is at toponium because $t\bar{t}$ decays to hadrons via three gluons. Since toponium is heavy (> 37.5 GeV/c^2) the three gluons will show up in most cases as three well defined jets. Application of a cluster algorithm will result in a large fraction of well-defined three cluster (jets) events. A study of this type was done[15] some while ago for $M_{t\bar{t}} = 30$ GeV/c^2. (The conclusions of this study are only strengthened by the fact that we know now that $M_{t\bar{t}} > 30$ GeV/c^2). Monte Carlo events were generated at 30 GeV for toponium and the continuum. We will characterize toponium as ggg and the continuum as $q\bar{q} + q\bar{q}g$, where q and g stand for quark and gluon respectively. The cluster frequency distributions obtained using the cluster algorithm are shown in Fig. 37. One sees that in the case of ggg the cluster algorithm reconstructs half the events as three jet events. It is shown in Ref. 15 that the assignment of particles to the jets by the cluster algorithm reproduces the produced jet assignments very well. Those events which are reconstructed as two jet events are those in which two of the gluon jets overlap. In the continuum the reconstructed number of three jet events is much smaller because only about 25% of the events are $q\bar{q}g$ (i.e., have a gluon of sufficient energy to warrant calling the final state a three parton state) and many of those have a large overlap between the gluon and the quark which radiated the gluon. These will be reconstructed as two cluster events. We then propose the following procedure to test whether quarks and gluons of the same (high) energy hadronize differently. Suppose one is running at $E_{c.m.} = 40 - 60$ GeV. In this case the continuum cross section is the same as the peak cross section for toponium (see Fig. 5). The first step in the test is to run at the peak of toponium and accumulate three jet events. Assuming $< \mathcal{L} >= 10^{31}\ cm^{-2}\ sec^{-2}$ and the cluster finding efficiencies from Fig. 37, one would get 18 ggg three jet events/day and 7 $q\bar{q}g$ three jet events per day; one would have a sample of three jet events in which the fastest jet had an energy of 14-18 GeV and was 70% "gluon rich." The second step is to run below toponium and accumulate three jet events. These would

accumulate at 7 events/day and the fastest jet would again have 14-18 GeV and be 100% quark. One would now compare the decay properties of the fastest jet on and off the toponium resonance. The obvious variables to test are the multiplicity and the $< p_T >$ for the jet particles relative to the reconstructed jet axis. The multiplicity should be $\sim$ twice as large and $< p_T >$ should be appreciably larger for the gluon jets relative to the quark jets. One would immediately be able to tell if gluons fragment differently than quarks. The advantage of this test is that no corrections are needed, no Monte Carlo simulations – one merely compares observed distributions.

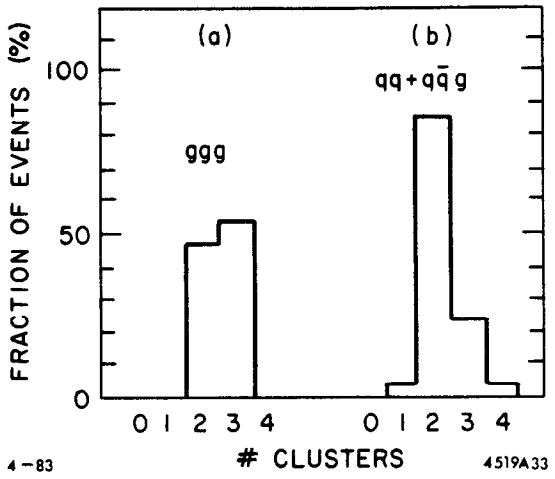

Fig. 37. The cluster frequency distributions for $e^+e^- \to ggg$ (a) and $e^+e^- \to q\bar{q} + q\bar{q}g$ (b) at $E_{c.m.} = 30$ GeV.

One could argue that a somewhat more formal test of the gluon self-coupling might be preferable. Such tests have been proposed and we choose as an example the method proposed in Ref. 33 by Koller et al. It involves looking at four jet events produced at toponium. In this case one would have dominant contributions from the two diagrams shown in Fig. 38. The authors argue that (a) is about four times more copious than (b) and hence an absence of the $g \to gg$ coupling required for (a) can be detected. We estimate that $\leq 10\%$ of the toponium hadronic decays will reconstruct as clear four cluster events. For $< \mathcal{L} >= 10^{31}\ cm^{-2}\ sec^{-1}$, this corresponds to a signal of 3 events/day. A one-year run under these conditions would suffice.

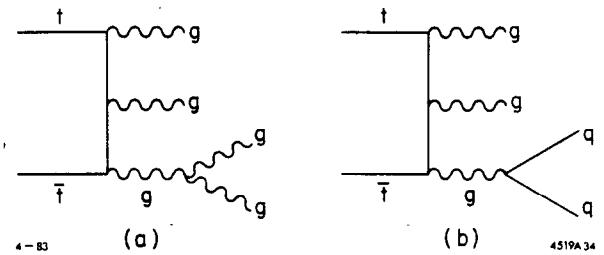

Fig. 38. The two dominant diagrams for producing four jet events at toponium.

There are two distinct four jet topologies which result and these are shown in Fig. 39. The authors suggest focusing on the Class B events which are about twice as plentiful as Class A events. Define the two jet group which has the smallest invariant mass as the slim jet side. The choice of the slim jet favors strongly the side where the $g \rightarrow gg$ or $g \rightarrow q\bar{q}$ branching occurred. Several variables show measurably different spectra for 38(a) and 38(b) and we show in Fig. 40 the distribution of $cos\theta_{ij}$ for the two possibilities. The angle θ_{ij} is the angle of the slim jet with respect to the overall four jet thrust axis defined in the rest frame of the slim jet. One sees that the $g \rightarrow gg$ process favors $cos\theta_{ij} \rightarrow 1$ whereas the $g \rightarrow qq$ is relatively flat. If the gluon self coupling were not present one would see it both in the yield and shape of the $cos\theta_{ij}$ plot. This method would seem promising. Other proposed probes for the gluon self-coupling include tests at the Z^0 (Ref. 34) and tests in the continuum (Ref. 35).

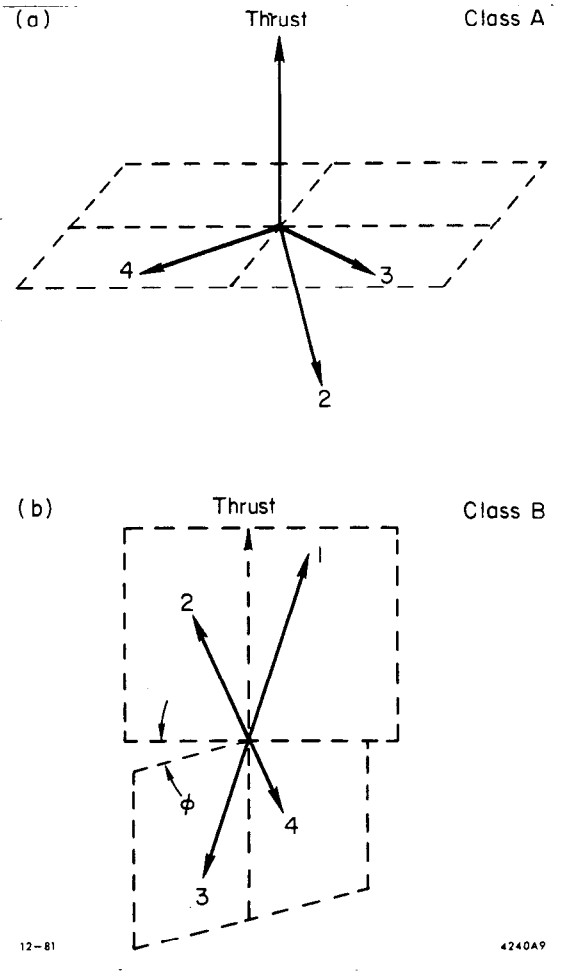

Fig. 39. Kinematic configuration for the class A and B events. In (a) the thrust axis will be along the momentum vector of one of the jets and the three other jets will be in the opposite hemisphere. In (b) there are two jets in each hemisphere.

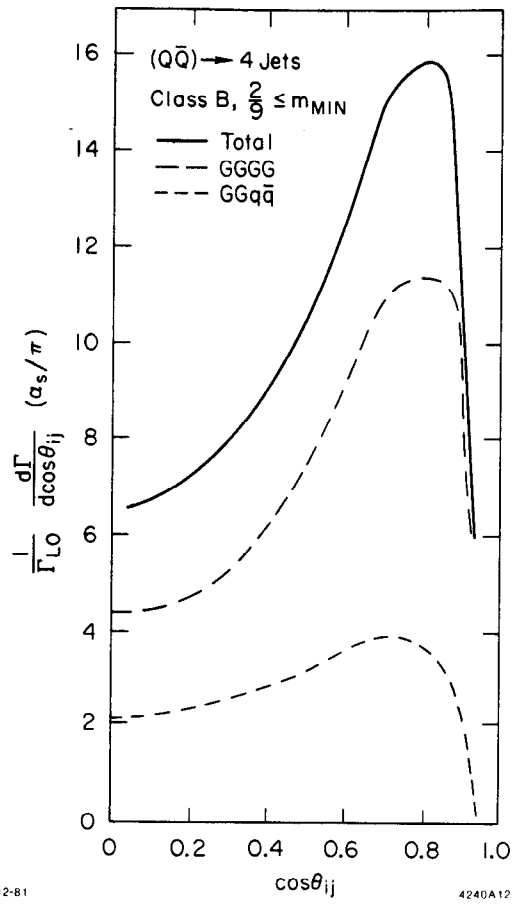

Fig. 40. Angular distribution of the two-jet system on the "slim" side of the event relative to the thrust axis. This angular distribution is evaluated in the two-jet center-of-mass.

Why not use PETRA/PEP gluon jets to study the difference between gluon and quark fragmentation? There are several problems with this approach. In general the three jet events do not have the softest jet well separated from the intermediate energy jet. This overlap of jets makes the measurement of jet energy, jet multiplicity and mean p_T very difficult. One only has a statistical assignment of the "gluon rich" jet and most of the gluons are soft. One would like to have high energy jets which were well measured with reliable particle assignments. Unfortunately, with PETRA/PEP type events one has a situation where the "gluon rich" jet is the softest and is the most poorly measured. If one asks for a high energy gluon one moves towards the configuration in which each parton carries $E_{c.m.}/3$. However, in this configuration the assignment of any jet to the gluon hypothesis is a purely random one, namely the odds are 1/3 for any jet you choose. It is the author's opinion that it will be very difficult at the present PETRA/PEP energy range to conclusively demonstrate that gluons fragment differently than quarks. Perhaps if PETRA can get a very large ($100pb^{-1}$) data set at $\geq$ 40 GeV it can be done.

Luckily there are people who disagree with the author's personal opinion! The JADE group[36] claim that they do see differences in the mean p_T between the soft jet (gluon rich) and intermediate energy jet (quark rich). There are, however, analyses[29,37] which claim to see no effect and the JADE results require confirmation or in the words of Braunschweig (Ref. 25), "... the effect seen by the JADE group needs further study."

4.5 Does α_s Run – And, If So, How do we "Clock" It?

The question posed above seems somewhat akin to measuring the progress of a snail using a watch calibrated in femtoseconds – the point being, of course, that α_s runs very slowly. Remembering the formula given in Sec. 3 and taking $n_f = 3$ and $\alpha_s[(30\ \text{GeV})^2] \equiv 0.17$ one finds

$E_{c.m.} = (\text{GeV})$	α_s
30	.170
93 (Z^0)	.156
140 (LEP II)	.150
300 (VLEPP I)	.140
1000 (VLEPP II)	.130

In order to understand how hard it is to see these small changes in α_s one should keep in mind that the typical errors in α_s coming from PEP/PETRA measurements are 0.02 statistical and 0.03 systematic. The present level of systematic errors is the difference in α_s at 30 and 300 GeV! So it will be very hard to measure the running coupling constant by raising $E_{c.m.}$.

Is there an alternative at present energies? Could we investigate the process whereby a quark evolves into a jet of hadrons and sample different values of Q^2 in the sense that early times $\Rightarrow$ short distances $\Rightarrow$ large Q^2? An analysis along these lines has been performed by the MARK II group.[38] The discussion is complicated and the interested reader is encouraged to consult the reference.

4.6 QUARK CONFINEMENT

Confinement was a direct consequence of the non-Abelian nature of QCD. The Fairbank et al[39] results indicate that free quarks exist and, while this result needs confirmation, we cannot ignore it simply because it makes us uncomfortable. What evidence do we have from e^+e^- experiments on the existence of free quarks? None have been seen and the limits taken from Ref. 13 are shown in Fig. 41. Searches are done for quark pair production and for inclusive quark production. Figure 41 shows the limits obtained for the cross section for these processes normalized to the point cross section. As we probe still higher energies, we must always remain vigilant and ensure that the new detector designs do not preclude searching for free quarks.

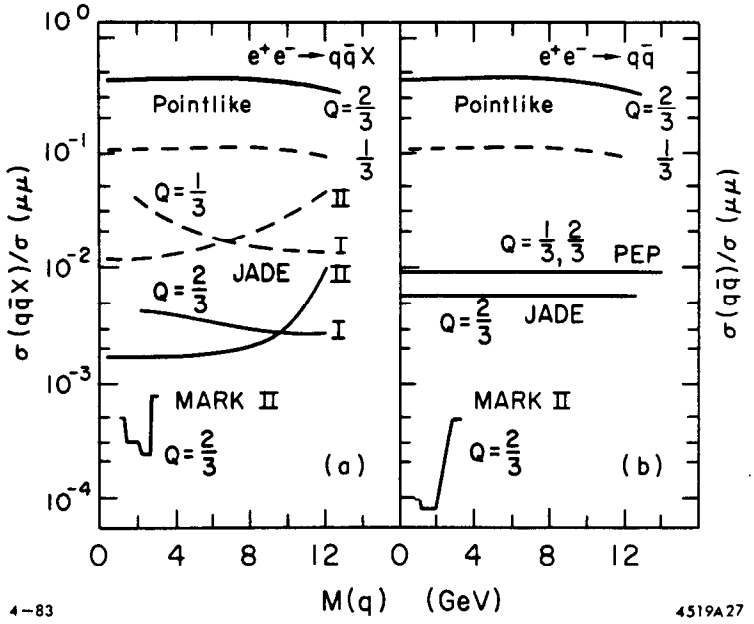

Fig. 41. Results from the e^+e^- quark search experiments is shown for the inclusive channel (a) and the exclusive channel (b). Shown are the upper limits for the production cross sections at the 90% confidence level. The two options I and II represent alternative models for obtaining corrected cross sections.

5. Simple Extensions of $SU(3) \wedge SU(2) \wedge U(1)$

5.1 Models With More Than One Higgs Doublet

The minimal version of the Weinberg-Salam model has a complex doublet of Higgs fields (Sec. 3). There are no theoretical reasons for excluding the introduction of more than one doublet of Higgs fields in the standard model. There are many instances of models which use two complex doublets. This alternative offers a possible solution to the strong CP problem, and is used in both supersymmetry models and $SU(5)$. In such models one has

$$\phi_1 = \begin{pmatrix} \phi_1^+ \\ \phi_1^0 \end{pmatrix} \ , \quad <\phi>_0 = V_1$$

$$\phi_2 = \begin{pmatrix} \phi_2^+ \\ \phi_2^0 \end{pmatrix} \ , \quad <\phi>_0 = V_2$$

where $V_1 + V_2 = V = \sqrt{2}\, \mathcal{G}_F$. When the spontaneous symmetry breaking occurs, three of the eight fields are eaten by the $W^\pm$ and Z^0 while five remain as physical fields. These result in two neutral bosons with scalar couplings to quarks and leptons (H_1^0, H_2^0), one neutral boson with pseudoscalar couplings (h^0) and two charged scalar bosons $(H^\pm)$. In some models h^0 is associated with the axion. In order to avoid flavor changing neutral currents, it is arranged that ϕ_1 gives mass to the charge $\frac{2}{3}$ quarks and ϕ_2 gives mass to the charge $\frac{1}{3}$ quarks. The couplings, as in the minimal model, are specified:

$$g_{fH_1} = \frac{1}{V_1} M_{u,c,t} \ , \quad g_{fH_2} = \frac{1}{V_2} M_{d,s,b} \ .$$

However the ratio $X \equiv V_1/V_2$ is not known. Since $M_c > M_s$ and $M_t > M_b$ it is surmised, but not necessary, that $V_1 > V_2$. We will assume for discussion of searches that $X \geq 1$ and that the charged Higgs scalars like to couple to the heaviest fermion pair available. By direct analogy with the $W^\pm$ sector, Kobayashi-Maskawa type mixing can occur in the $H^\pm$ sector. We have no knowledge of how large this mixing might be but we will assume here that the mixing is small.

Why do we choose only isodoublets for the Higgs fields? There are several reasons – two are given here. Higgs fields with weak isospin $\neq \frac{1}{2}$ (triplets, etc.) cannot participate in the generation of fermion masses. They also upset the successful theoretical

prediction of the standard model for the ratio of the strength of charged and neutral currents. Suppose we introduce a triplet of Higgs fields

$$\eta = \begin{pmatrix} \eta^+ \\ \eta^0 \\ \eta^- \end{pmatrix} \quad <\eta>_0 = Y \ .$$

Following the symmetry breaking one finds that $<\eta>_0$ contributes extra mass to the $W^\pm$ and

$$\rho = \frac{M_{W^\pm}^2}{M_{Z^0}^2 cos^2\theta_W} = 1 + \frac{4Y^2}{V^2} > 1 \ .$$

In the standard model $\rho = 1$ and this is well confirmed by all the data.[9]

We have no theoretical guidance for the $H^\pm$ mass. We expect that

$$\left.\begin{array}{l} H^\pm \to c\bar{s} \text{ or } c\bar{b} \\ \to \tau\nu \end{array}\right\} \quad M_{H^\pm} < M_t$$

$$H^\pm \to t\bar{b} \qquad M_{H^\pm} > M_t \ .$$

Pairs of charged Higgs particles will be produced in e^+e^- interactions, $e^+e^- \to H^+H^-$, with a cross section characteristic of scalars:

$$\frac{d\sigma}{d\ cos\theta} = \frac{1}{4}\ \sigma_{\mu\mu}\ \beta_H^3 sin^2\theta \tag{4}$$

$$R_{H^+H^-} = \frac{\sigma_{H^+H^-}}{\sigma_{\mu\mu}} = \frac{1}{4}\ \beta_H^3 \tag{5}$$

where β_H is the velocity of the $H^\pm$. $R_{H^+H^-}$ is too small a contribution to permit a confident discovery. The angular distribution is distinctive, but it will not be easy to see a small (1/16) admixture of $sin^2\theta$ superposed on a $cos^2\theta$ distribution. However this test should be performed by the PEP and PETRA groups. A more dramatic signature is the modification of heavy quark decay by the charged Higgs. This decay can proceed via $H^\pm$ in direct analogy with the standard $W^\pm$ diagram (see Fig. 42). The $H^\pm$ diagram dominates the $W^\pm$ for the assumption that there is small mixing in the Higgs sector. In the decays $Q \to H^\pm q$ and $Q \to W^\pm q$ the ratio $\Gamma(H^\pm q)/\Gamma(W^\pm q)$

ranges from 10^3 to 60 as M_Q ranges from 15 to 80 GeV/c^2. So if $M_{H\pm} < M_c$, M_τ the D^0 and τ would have considerably shorter lifetimes than those measured. We may conclude then that $M_{H\pm} \geq 1.8$ GeV/c^2. We can obtain a larger limit on $M_{H\pm}$ from B decay. There are two possibilities (in the conventional lore considered in these lectures) for the decay of bottom via $H^\pm$. These are shown in Fig. 43. They offer two limiting cases: (a) $H^\pm \to c\bar{s}$ only in which case we will see no leptons and lots of charged energy in B decays and (b) $H^\pm \to \tau^\pm\nu$ only in which case we will see a lot of leptons and substantial missing energy in B decays. The CLEO experiment[31b] has looked for $H^\pm$ and shown in Fig. 44 is a plot of the observed charged energy fraction versus the lepton branching fraction. The data convincingly rule out the possibility that B decay is mediated by $H^\pm$. We conclude that $M_{H\pm} \geq 5$ GeV/c^2. To obtain larger limits we must consider the data from PEP and PETRA.

Fig. 42. The decay of a heavy quark in the standard model (a) and in the extended standard model which contains charged Higgs particles (b).

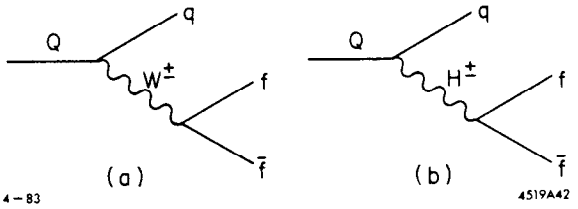

Fig. 43. If b quark decay was mediated by $H^\pm$, the prominent decay modes (for $M_{H\pm} < M_t$) will be those shown above.

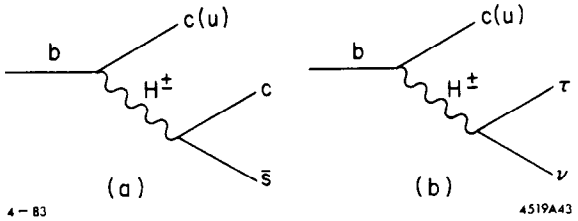

Three event configurations are looked for. They are

$$e^+e^- \to H^+ H^- \begin{cases} \to \tau^- \nu_\tau \\ \to \tau^+ \bar{\nu}_\tau \end{cases}, \tag{6}$$

$$e^+e^- \to H^+ H^- \begin{cases} \to c\bar{s} \\ \to \tau^+ \bar{\nu}_\tau \end{cases} \quad \text{and} \tag{7}$$

$$e^+e^- \to H^+ H^- \begin{cases} \to c\bar{s} + c\bar{b} \\ \to c\bar{s} + c\bar{b} \end{cases}. \tag{8}$$

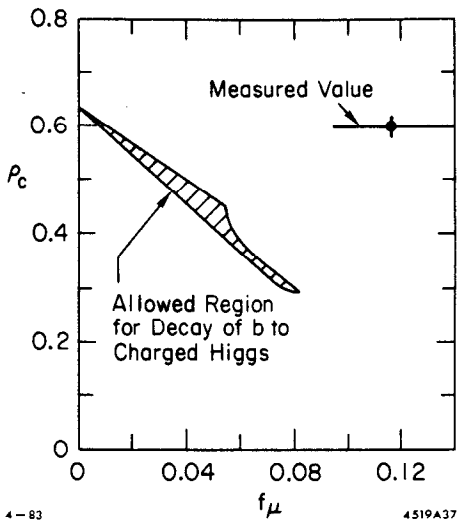

Fig. 44. Data from the CLEO experiment showing the measured charged energy fraction (ρ_c) versus the fraction of muons. The allowed region for the decay of b via a charged Higgs is shown along with the measured value.

These searches have been performed by many groups[40]: MARK II (6) and (7), TASSO (8), JADE (7), CELLO (6) and MARK J (6). The analyses involve choosing event topologies consistent with (6)-(8) and asking whether there exist events in excess of those resulting from conventional sources. The production rate and angular distribution is assumed to be given by (4) and (5). Monte Carlo simulations of the Higgs decays are used with variable $M_{H^\pm}$ to obtain limits. In the searches (6) and (7) it is assumed that the branching fractions for $H^\pm \to \tau\nu(B_\tau)$ and the branching fraction for $H^\pm \to c\bar{s}(B_{c\bar{s}})$ sum to one: $B_\tau + B_{c\bar{s}} = 1$. The analyses differ in detail; we use the MARK II analysis as an example of (6) and (7). Transverse momentum (p_T) is used as a measure of mass. We can think of the event topologies for (6) and (7) as being characterized by two hemispheres each containing the decay products of one of the parent scalars. An axis can be defined so that the p_T of both sets of decay particles is the same. This is a measure of the p_T in the parent decay. Figure 45a shows this p_T spectrum for events chosen to be representative of process (6). The conventional source for these events is $e^+e^- \to \tau^+\tau^-$ and we see that the absolutely normalized expectation for $\tau^+\tau^-$ production accounts very well for the data. There is no room for appreciable H^+H^- production. Using Monte Carlo predictions of the type shown in Fig. 45a for a 7 GeV/c^2 $H^\pm$, limits on $M_{H^\pm}$ can be obtained as a function of B_τ. These limits are shown as II in Fig. 46a. A similar analysis is done for (7), the results are shown in Fig. 45b and 46a. The results of the PETRA analysis for (6) and (7) are shown in Fig. 46b. PETRA runs at a higher $E_{c.m.}$ and hence the PETRA experiments

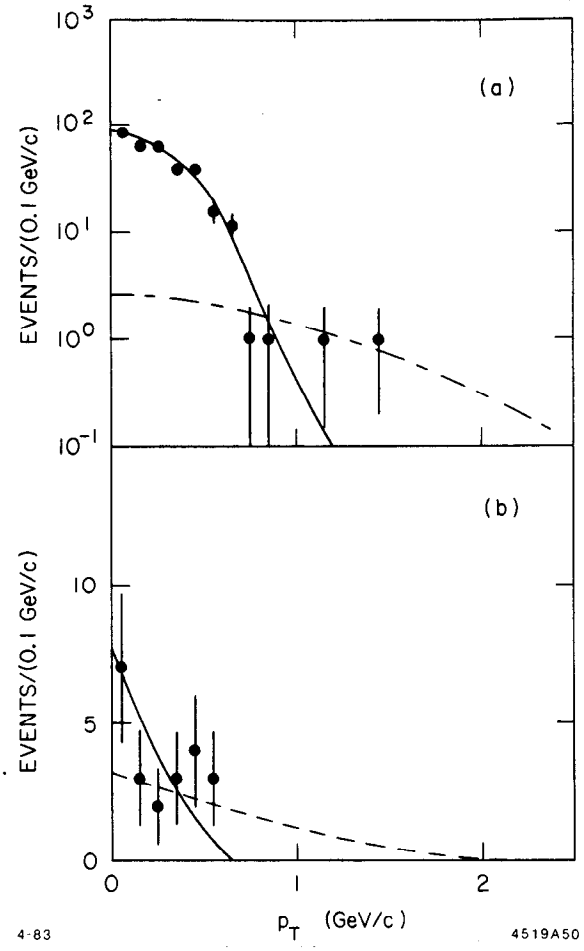

Fig. 45. (a) p_T distribution for τ-pair events. The solid curve is the expectation for normal τ-pair production. The dashed curve is the expectation for a Higgs with mass 7 GeV/c^2 and $B(H \rightarrow \tau\nu_\tau) = 0.5$.
(b) p_T distribution for events with one prong opposite a multiprong jet. The solid curve is the prediction of the hadron Monte Carlo program normalized to the data. The dashed curve is the expectation for a Higgs with mass 7 GeV/c^2 and $B(H \rightarrow hadrons) = 1 - B(H \rightarrow \tau\nu_\tau) = 0.5$.

are able to place more stringent limits on $M_{H\pm}$. The study of (8) is much more difficult because the event topology will look very similar to the continuum $e^+e^- \rightarrow$ hadrons. TASSO[40] has done a four jet analysis in which they have found a kinematic separation between the scalar events and the continuum events. The results of this study are shown in Fig. 46c. Taking all the results in Fig. 46, it appears unlikely that there exists a charged scalar (with the properties described in this chapter) having a mass within the range of 5-13 GeV/c^2. Combining the τ and D^0 lifetime measurements, the CLEO, PEP and PETRA measurements it seems probable that $M_{H\pm} \geq 13$ GeV/c^2. As the energy at PETRA is raised, so will the limits on $M_{H\pm}$. When PETRA reaches $E_{c.m.} = 46$ GeV the experiments should have sensitivity to 21-22 GeV/c^2 in $M_{H\pm}$.

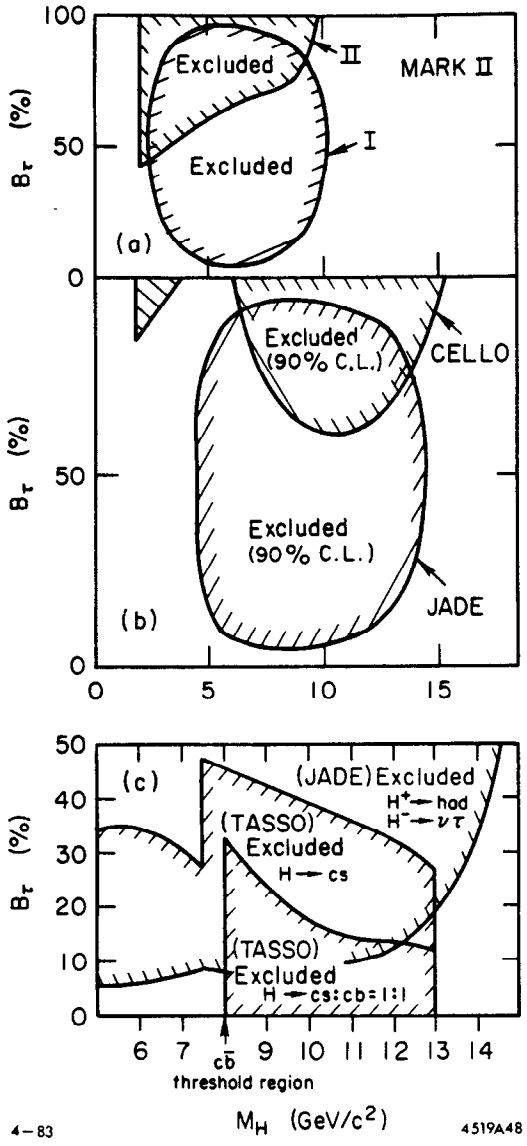

Fig. 46. Limit on $B(H^\pm \to \tau^\pm\nu)$ are shown as a function of $M_{H^\pm}$. The data come from[40] MARK II (a), JADE and CELLO (b) and and TASSO (c). The models assumed in these analyses have $B(H^\pm \to \tau^\pm\nu) + B(H^\pm \to hadrons) = 1$.

Toponium is a good place to look for charged Higgs particles. If $M_{H^\pm} < M_{t\bar{t}}/2$ the diagram shown in Fig. 47 will dominate all other decay processes for toponium. This will make the toponium resonance much broader. At $M_{t\bar{t}} = 60$ GeV, Γ_{tot} is expected to be $\sim$ 10 MeV if the process in Fig. 47 is dominant. The TRISTAN machine width is predicted to be $\sim$ 60 MeV and even if charged Higgs dominate the decays of toponium, the machine resolution will dominate the measured width. The events however would be very distinctive relative to the expected decay topology $t\bar{t} \to ggg$. Firstly the events would not be planar and secondly there would be a lot of multilepton events. It would be an easy task to search for this possibility which offers the potential for achieving sensitivity up to $M_{H^\pm} \leq M_{t\bar{t}}/2$.

Fig. 47. The decay of toponium in the presence of a charged scalar particle.

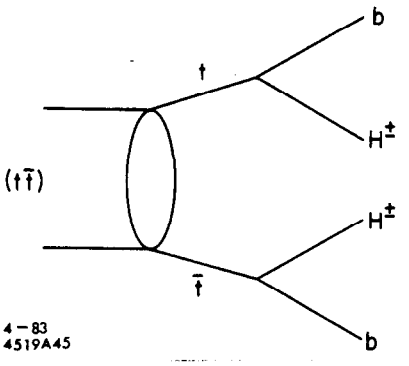

Unfortunately the Z^0 will not be a good place to look for charged Higgs particles. The coupling of the Z^0 to charged scalars is small as shown in Fig. 48. While the hadronic cross section increases by about 10^3 at the Z^0 (relative to the e^+e^- continuum), pair production of charged Higgs particles increases by <10.

Fig. 48. The cross section for the process $e^+e^- \rightarrow H^+H^-$ as a function of $E_{c.m.}$.

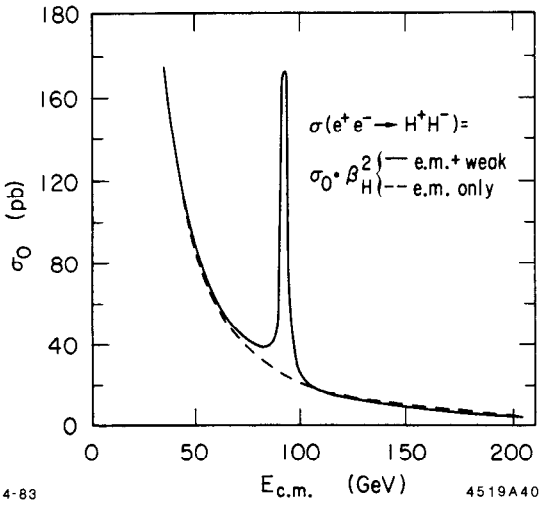

If the charged Higgs particle is more massive than $M_{t\bar{t}}/2$, we will have to search for it in the continuum. This will be very difficult unless there is another (new) heavy lepton which dominates the decays of the $H^{\pm}$. In the absence of the clean signature this new heavy lepton would afford, the events coming from pair production of $H^{\pm}$ will be very difficult to disentangle from the continuum jet events.

5.2 MODELS WITH EXTENDED ELECTROWEAK GAUGE GROUPS:

$SU(2) \wedge U(1) \wedge \mathcal{G}$.

At low Q^2, the effective Hamiltonian of the standard model for charged current interactions is given by

$$H_{cc} = \frac{4\mathcal{G}_F}{\sqrt{2}} J_\mu^+ J_\mu^-$$

and for neutral current interactions by

$$H_{NC} = -\frac{e^2}{q^2} J_{em}^2 + \frac{4\mathcal{G}_F}{\sqrt{2}} \left\{ (J^3 - sin^2\theta_W J_{em})^2 \right\}$$

where (J^+, J^-, J^3) form the weak isospin current. The success of the standard model at low energies is testament to the validity of this current-current description. Neither neutrino scattering experiments nor the *e-d* parity violation experiment probe the electromagnetic part of the weak current. Hence we can add to H_{NC}

$$H'_{NC} = -\frac{e^2}{q^2} J_{em}^2 + \frac{4\mathcal{G}_F}{\sqrt{2}} \{ (J^3 - sin^2\theta_W J_{em})^2 + C J_{em}^2 \}$$

without conflicting any of the low energy experimental data. The only low energy bound for C is $C < 4$ which comes from measurements of the anomalous magnetic moment of the muon.

The lepton pair charge asymmetry measurements at PETRA and PEP probe the term CJ_{em}^2 via the interference of the weak and electromagnetic propagators. We will return to the measurements at the end of this section. The freedom implied by the addition of the term CJ_{em}^2 permits models which extend the electroweak gauge group to $SU(2) \wedge U(1) \wedge \mathcal{G}$. Examples of such models are $SU(2) \wedge U(1) \wedge U(1)'$ (Ref. 41), $SU(2) \wedge U(1) \wedge SU(2)'$ (Ref. 42) and $SU(2)_L \wedge SU(2)_R \wedge U(1)$ (Ref. 43). The common feature of these models is the presence of two Z^0's with $M_{Z_1} < M_{Z^0} < M_{Z_2}$ where M_{Z^0} is the mass of the Z^0 in the standard model. The reason why one gets two energy levels is that CJ_{em}^2 can be thought of as a perturbation and this perturbation splits the single energy level (M_{Z^0}). We discuss briefly the models for which $\mathcal{G} = U(1)$ and $SU(2)$.

In the models in which $\mathcal{G} = U(2)$,[41] all fermions transform under $SU(2) \wedge U(1)$ in the usual manner and they are invariant under $U(1)'$. The spontaneous symmetry breaking is achieved using a pair of complex Higgs fields (see Sec. 5.1). The Higgs field ϕ_1 follows the standard model prescription. However, ϕ_2, which is invariant under $SU(2)$, has non-trivial transformations under $U(1) \wedge U(1)'$. Hence we recover the same $W^{\pm}$ structure as in the standard model. However ϕ_2 gives rise to an additional heavy neutral boson which can be associated with $U(1)'$. We thus obtain

for $U(1)$

$$(e^-, \nu_e) \qquad \begin{pmatrix} V_0 & 0 \\ 0 & V_0 \end{pmatrix} \begin{pmatrix} e^- \\ \nu_e \end{pmatrix}$$

for $SU(2)$

$$(e^-, \nu_e) \qquad \begin{pmatrix} W^0 & W^{-1} \\ W^+ & W^0 \end{pmatrix} \begin{pmatrix} e^- \\ \nu_e \end{pmatrix}$$

and for $U(1)'$

$$(e^-, \nu_e) \qquad \begin{pmatrix} V_0' & 0 \\ 0 & V_0' \end{pmatrix} \begin{pmatrix} e^- \\ \nu_e \end{pmatrix}$$

Standard Model

$$(\gamma, Z^0) = \begin{pmatrix} cos\theta & -sin\theta_W \\ sin\theta_W & cos\theta_W \end{pmatrix} \begin{pmatrix} V^0 \\ W^0 \end{pmatrix} ;$$

one parameter $sin^2\theta_W$

$SU(2) \wedge U(1) \wedge U(1)'$

$$(\gamma, Z_1, Z_2) = (3 \times 3) \begin{pmatrix} V_0 \\ V_o' \\ W_0 \end{pmatrix} ;$$

three parameters .

The three parameters of $SU(2) \wedge U(1) \wedge U(1)'$ can be taken as $sin^2\theta_W$, M_1 and M_2. The parameter C is given by

$$C(\mathcal{G} = U(1)) = cos^4\theta_W \left(\frac{M_{Z^0}^2}{M_1^2} - 1\right)\left(\frac{M_{Z^0}^2}{M_1^2} - 1\right)$$

so as either $M_{1,2} \to M_{Z^0}$ we recover the standard model with $C = 0$.

In the model with $\mathcal{G} = SU(2)$[42] one goes through a similar procedure but in this instance ϕ_2 has non-trivial transformations under $SU(2) \wedge SU(2)'$. Again one obtains two neutral heavy bosons. In this model

$$C(\mathcal{G} = SU(2)) = sin^2\theta_W \left(\frac{M_{Z^0}^2}{M_1^2} - 1\right)\left(\frac{M_{Z^0}^2}{M_2^2} - 1\right)$$

and again $C = 0$ as $M_{1,2} \to M_{Z^0}$.

From PETRA we obtain limits on C via the measurements of the lepton charge asymmetries. The asymmetry data is fit using an interaction which contains the term CJ^2_{em}. The limits obtained from the PETRA groups[18] are shown in Table 6.

Table 6. Limits on C.

Group	95% C.L. for C
CELLO	< 0.031
JADE	< 0.039
MARK J	< 0.027
PLUTO	< 0.060
TASSO	< 0.030

Figure 49 shows the bounds on M_1 and M_2 obtained from the MARK J measurements. For $\mathcal{G} = U(1)$, the 95% confidence level limit requires that one of the two neutral bosons have a mass very close to M_{Z^0}. The model in which $\mathcal{G} = SU(2)$ is not as tightly constrained because $C \propto sin^4\theta_W$ as opposed to $C \propto cos^4\theta_W$ in the model with $\mathcal{G} = U(1)$.

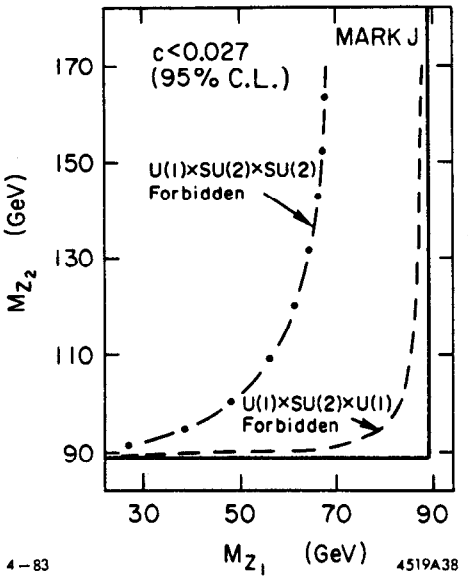

Fig. 49. Forbidden regions of the M_{Z_1}, M_{Z_2} plot are shown for the two possibilities $\mathcal{G} = U(1)$ and $\mathcal{G} = SU(2)$. The region to the left of the curves is forbidden.

What are the prospects of sorting out the correct electroweak gauge group as we go up in $E_{c.m.}$? We can imagine two scenarios. In the first scenario there is no Z^0

near 93 GeV/c^2. In this case we will have to move down to lower energies searching for Z_1. One would presumably benefit in such a search from the fact that there will be a substantial radiative tail for the Z_1 which will show up in a measurement of R. In the second scenario M_1 would be very close to M_{Z^0} with M_2 substantially larger than M_{Z^0}. What can be done in such a situation? This is thoroughly discussed in the SLC workshop[5b] and we borrow here liberally from this discussion (pages 44-52). The trick to sorting out the latter scenario is the longitudinal asymmetry measurement discussed in Sec. 4.2. If one looks back at the form of the modified neutral current Hamiltonian, one sees that, in essence, the addition of the term CJ^2_{em} has the effect of modifying $sin^2\theta_W$. The longitudinal asymmetry (A_L) is exceedingly sensitive to $sin^2\theta_W$ as we see in Fig. 50. Shown in Fig. 50 is A_L as a function of $E_{c.m.}$ for the standard model and for $SU(2) \wedge U(1) \wedge U(1)'$ in which $sin^2\theta_W$ is taken to be 0.22 (in agreement with the world average[9] $sin^2\theta_W = 0.230 \pm 0.015$). Running at the Z^0 pole one would easily see the deviation from the standard model. However one will have

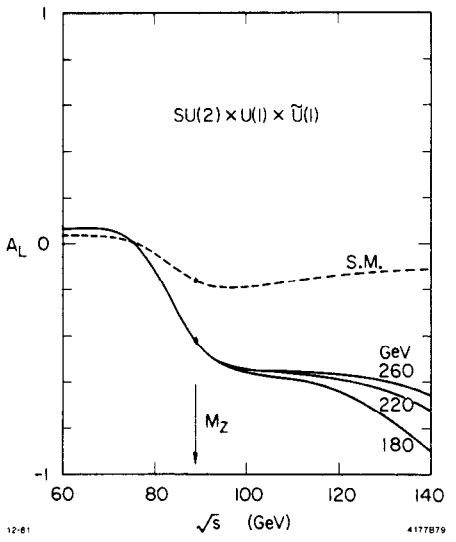

Fig. 50. The longitudinal lepton charge asymmetry is shown as a function of $E_{c.m.}$ for the standard model and $SU(2) \wedge U(1) \wedge U(1)'$. In the latter case curves for different M_{Z_2} are shown. M_{Z_1} is assumed to be at M_{Z^0} and $sin^2\theta_W = 0.22$.

to run at a substantially higher $E_{c.m.}$ in order to get sensitivity to M_2. Although not discussed here in detail, we show the sensitivity of A_L to tests for the model $SU(2)_L \wedge SU(2)_R \wedge U(1)$.[43] Figure 51 shows A_L as a function of $E_{c.m.}$ for the standard model and the left-right symmetric model. In this case running at the nominal Z^0 mass can distinguish the extended model from the standard model and yield the mass of the second heavy boson. This is shown more explicitly in Fig. 51b. We again see

how important longitudinally polarized electrons will be at the Z^0. We can conclude by saying that with the benefit of such polarized beams, considerable sensitivity to the electroweak gauge group can be obtained by running at the nominal Z^0 mass.

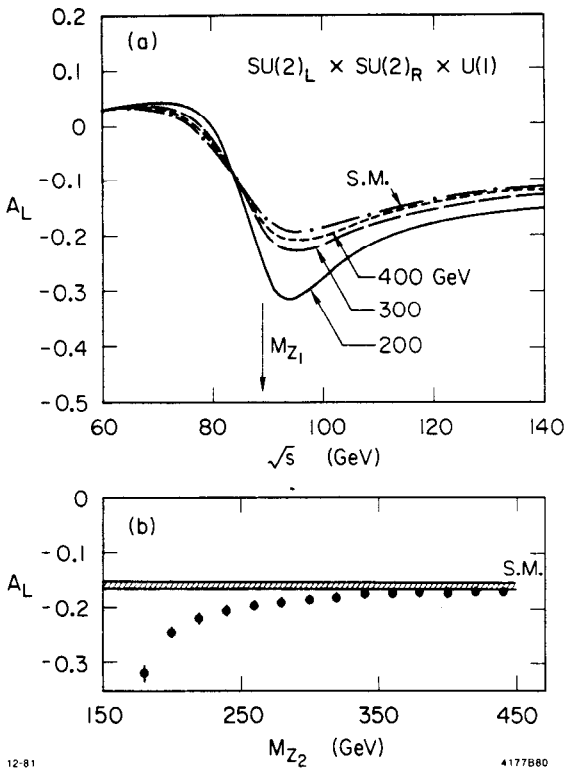

Fig. 51. (a) The longitudinal lepton charge asymmetry is shown as a function of $E_{c.m.}$ for the standard model and $SU(2)_L \wedge SU(2)_R \wedge U(1)$. Curves of different M_{Z_2} are shown for the latter model. The sensitivity to M_{Z_2} is shown on (b) when the data are accumulated at an energy of M_{Z^0}.

5.3 Models Without a Top Quark

The top quark has not been seen. This has led many people to speculate that maybe the top quark doesn't exist. Models have been constructed in which the left-handed b quark is a singlet; the four lower mass quarks retain their standard left-handed doublet assignment. These models are listed and discussed by Kane[44] and Kane and Peskin[44]. All the models discussed by Kane and Peskin have the common feature of substantial flavor changing neutral currents, which in particular lead to modifications of B decay. Kane and Peskin show that for all models there is a large rate for B's to decay to dileptons and quantitatively

$$r = \frac{\Gamma(B \to X\ell^+\ell^-)}{\Gamma(B \to X\nu\ell)} > 0.12 \ .$$

The CLEO experiment[31b] has looked for these dilepton events. They find ten such events (on 4S) where they expect twelve from conventional sources. This allows them

to set a limit

$$R < 0.08 \quad (90\%\ C.L.)$$

This measurement rules out all these models. More recently Peskin and Tye[45] have invented a model which suppresses the flavor changing neutral currents. The model has a most unnatural assignment of quarks:

$$\begin{pmatrix} u \\ d' \end{pmatrix}_L , \begin{pmatrix} c \\ s' \end{pmatrix}_L , \begin{pmatrix} c \\ b \end{pmatrix}_R \quad u_R, d_R, s_R, b_L \ .$$

However it cannot be ruled out by the present data. Possible future avenues are (a) at the Z^0 the charm axial-vector coupling constant will be zero and (b) the B will have a substantially shorter lifetime (factor of 10) than in the standard model. To test (a) is very hard – one would have to tag charm jets and measure the charm quark asymmetry.

5.4 More Generations – The Generation Puzzle

The discovery of the τ and the b quark has led to a very beautiful symmetry between the quark and lepton sectors. Nature at present appears to have three generations of both quarks and leptons. While this symmetry is indeed attractive, we are led to an obvious question – why three generations? Why not five or ten? We readily understand the need for one generation – our very being is dependent on it. But more than one generation seems superfluous and it is interesting to speculate on why nature chose to replicate itself in this strange way.

The distinguishing generation element is mass – successive generations have higher masses. A perfectly defensible reason why we see three generations then is that the energy of our machines is not sufficient to yield the next generation(s). The prospect of higher energy machines implies more quarks and leptons. We may go to our theoretical friends and ask them where we need to look; where will the next generation appear? The answer is that none of the current theories understands the generation puzzle and no mass predictions exist. Bjorken, in 1978, contemplated the fermion mass spectrum and mused that the mass of the next charged lepton would be at $\simeq$ 10 GeV/c^2 and the mass of the top quark would be $\simeq$ 27 GeV/c^2. The former is violated by the PETRA and PEP limits, so we see that our guide will have to be experiment.

How do we search for new flavors? There are three obvious possibilities

1. Search for a new charged lepton, $L^{\pm}$,
2. Search for a new $Q = -\frac{1}{3}$ quark, and
3. Search for more ν's.

We do not include searches for $Q = \frac{2}{3}$ quarks because if such a quark were found, it would satisfy our need for the top quark. Consider the search for $L^{\pm}$. The $W^{\pm}$ which mediate the decays of $L^{\pm}$, is democratic with respect to fermion coupling strengths. Allowing for three quark colors we have

$$B(L^{\pm} \rightarrow \ell^{\pm}\nu\nu) = \frac{1}{12} = 8\%$$

and

$$B(L^{\pm} \rightarrow hadrons) = 76\% \quad .$$

(These numbers will be modified slightly by QCD corrections but, for the argument being made here, these small modifications are unimportant.) We will therefore be able to use the standard low multiplicity searches for $L^{\pm}$ which will be pair produced in e^+e^- interaction with $R = \beta_L(3-\beta_L^2)/2$. Backgrounds are small because the $< n >_{charge}$ is large for the hadronic events. As an example at TRISTAN assuming $E_{c.m.} = 60$ GeV, $< \mathcal{L} >= 10^{31}\ cm^{-2}\ sec^{-1}$ one will have 20 L^+L^- events produced/day ($\beta_L = 1$) of which five events/day would have the topology of a single lepton in one hemisphere and ≥ 3 charged hadrons in the other hemisphere. Such a signal would be hard to miss. As $E_{c.m.}$ is raised, the searches will be rate limited and a high luminosity will be required. The rate goes like $E_{c.m.}^{-2}$. However at the Z^0 there will be plenty of rate with $B(Z^0 \rightarrow L^+L^-) = 3\%$. For these searches one has sensitivity up to $E_{c.m.}/2$.

Searches of this kind have been done at PETRA and PEP. The limits for sequential charged heavy leptons appear in Table 7.

Table 7. Limits on Sequential Heavy Leptons

Experiment	95% C.L. Lower Limit
JADE	18.1
MARK J	16.0
PLUTO	14.5
TASSO	15.5
MAC	14.0
MARK II	13.8

By the end of 1983, PETRA will have sensitivity to $M_{L^{\pm}} \simeq 23$ GeV/c^2.

How do we search for a $Q = -\frac{1}{3}$ quark? The change in R is $\frac{1}{3}$ which is too small to see given the present accuracy of R measurements. The new quark will be heavy and so event shapes will be a useful indicator. The presence of a new quark will be signalled by the onset of spherical, low thrust events. The signal is distinctive, but the rate is still low. The searches performed at PETRA indicate how such searches are made. Figure 52 shows the thrust for hadronic events containing a muon in the MARK J detector. The muon tag is used to enhance the heavy quark decay fraction. Shown on the plot is the expected yield for the five known quarks and for the five known quarks plus a charge $-\frac{1}{3}$ quark. The mass limit for charge $-\frac{1}{3}$ quarks obtained by the PETRA groups[13] is $M_{-\frac{1}{3}} > 15$ GeV/c^2. These kinds of shape analysis searches can be continued as $E_{c.m.}$ is raised. However, it takes a considerable amount of data (the PETRA limits come from data sets of $\sim 50 pb^{-1}$) to achieve good sensitivity and hence the searches require high luminosity machines.

At the Z^0, there is plenty of rate. A shape analysis akin to that discussed in Sec. 4.1 would very quickly signal a new heavy flavor. The question would then be is it a charge $-\frac{1}{3}$ or $\frac{2}{3}$ quark? Two possibilities come to mind for deciding. Because the weak coupling contants differ (see Sec. 3) for the two quark species, the production rate at the Z^0 differs. The difference is about 20% and if there was nothing else new contributing to the Z^0 total decay rate, it would probably be possible to make an assignment of the quark charge based on the event rate of the new flavor. The other alternative would be to measure the charge or longitudinal asymmetry which is

sensitive to the weak coupling constants. Running at the Z^0 provides sensitivity of $M_{-\frac{1}{3}} \leq M_{Z^0}/2$.

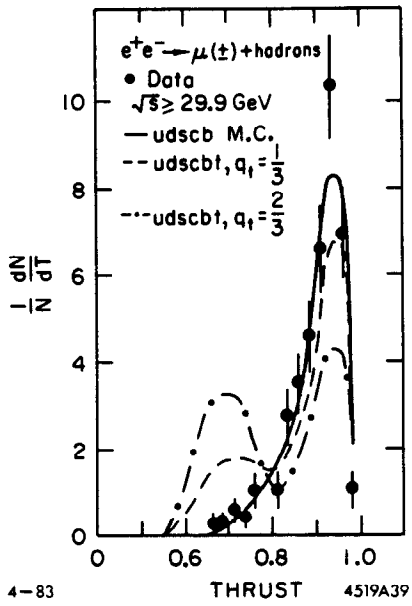

Fig. 52. The data of MARK J show the hadron thrust for hadronic events which contain a muon. Three alternative Monte Carlo options are shown. This measurement permits the MARK J to set limits on the presence of a charge $-\frac{1}{3}$ quark.

The third option for searching for new flavors involves counting the number of ν species. This can be done by measuring the width of the Z^0:

$$\Gamma_{Z^0} = \frac{\mathcal{G}_F M_{Z^0}^3}{\sqrt{2}\ 24\pi} \left\{ 2N_\nu + [1 + (1 - 4\ sin^2\theta_W)^2]\, N_\ell \right.$$
$$+ 3\left[1 + (1 - \frac{8}{3} sin^2\theta_W)^2\right] N_{\frac{2}{3}}$$
$$\left. + 3\left[1 + (1 - \frac{4}{3} sin^2\theta_W)^2\right] N_{-\frac{1}{3}} \right\}$$

where N_ℓ = number of charged leptons, N_α = number of quarks with charge α and N_ν = number of neutrino flavors. Each additional neutrino flavor contributes

$$\frac{\mathcal{G}_F M_{Z^0}^3}{\sqrt{2}\ 12\pi} \simeq 160\,\text{MeV}$$

to Γ_{Z^0}. In the standard model, $\Gamma_{Z^0} = 2.5$ GeV. In order to observe a 3σ effect implies measuring Γ_{Z^0} to $\simeq 2\%$. This will be a very difficult task because the measured width will have to be corrected for complicated radiative effects, beam dynamics (machine energy spread, stability, etc.). G. Barbiellini et al.,[47] discuss running above the Z^0 searching for events of the type

$$e^+e^- \rightarrow \gamma Z^0 \quad \hookrightarrow \nu\bar{\nu} \tag{9}$$

The signature for these events would be a single hard photon. The main background comes from $e^+e^- \rightarrow e^+e^-\gamma$. However, if one can cover the solid angle with electromagnetic calorimetry down to $\sim 6^o$ of the beamline, then the γ from $e^+e^-\gamma$ must be accompanied in the detector by at least one of the $e^{\pm}$. The cross section for (9) is given in the standard model by

$$\frac{d^2\sigma}{dxdy} = \frac{\mathcal{G}_F^2\, \alpha\, E_{c.m.}^2 (1-x)\left[(1-\frac{x}{1})^2 + \frac{x^2y^2}{4}\right]}{6\pi^2\ x(1-y^2)}$$

$$\times \left\{ \frac{N_\nu(g_V^2+g_A^2) + 2(g_V+g_A)\left[1 - E_{c.m.}^2(1-x)M_{Z^0}^2\right] + 2}{\left[1 - E_{c.m.}^2 \frac{(1-x)}{M_{Z^0}^2}\right] + \Gamma_{Z^0}^2 M_{Z^0}^2} \right\}$$

where $x = \frac{E_\gamma}{E_{c.m.}}$ and $y = cos\theta_\gamma$. One chooses $E_{c.m.}$ so as to optimize the signal to noise. Figure 53 is taken from Barbiellini et al., showing the photon yield resulting from a choice of $E_{c.m.} = 105$ GeV. Each additional ν flavor contributes a change of $0.01 nb^{-1}$. A 60 day run at $< \mathcal{L} >= 2 \times 10^{30}\ cm^{-2}\ sec^{-1}$ will produce 300 events with E_γ within 2.5 GeV of the peak. If SLC or LEP can achieve their design luminosity, then this ν counting experiment will be a realistic possibility. It should be pointed out that in fact the experiment described above actually counts the number of neutral, weakly coupled objects some of which might not be neutrinos. An example of other possible sources are supersymmetry particles (see next section). The detector required for this experiment is one which has continuous electromagnetic coverage down to angles of 6^o. This coverage can be crude in the forward directions (small angles) since the signal photon gives adequate rate if $160^o > \theta > 20^o$. An energy resolution of $\sigma_E/E \leq 15\% / \sqrt{E}$ is required. Charged tracking is needed in the region $160^o >$

$\theta > 20^o$ to ensure that the energy deposited in the calorimeter was that of a neutral particle. These requirements are not very stringent and it will not be difficult for the general purpose detectors at LEP and SLC to ensure that they will be able to make this important measurement.

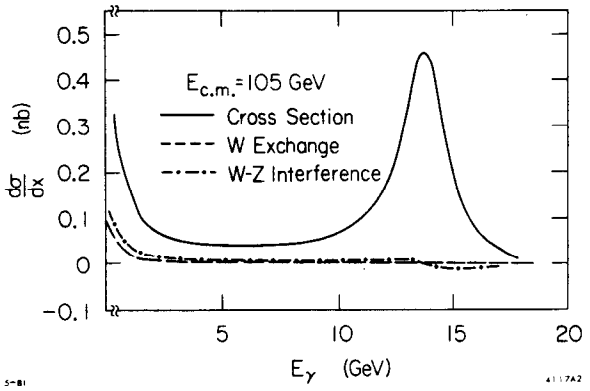

Fig. 53. The differential cross section $d\sigma/dx$ ($x = 2E_\gamma/E_{c.m.}$) is shown as a function of E_γ for the process $e^+e^- \to \gamma\nu\bar{\nu}$. The calculation assumes $E_{c.m.} = 105$ GeV.

6. Models Which Avoid the Gauge Hierarchy Problem

There are many different ways to state the so called "gauge hierarchy problem." The Higgs mechanism sets a mass scale – the electroweak scale – in a most unnatural way because the process requires remarkably fine tuning. Stated another way, the radiative corrections to the Higgs mass, shown in Fig. 54, are quadratically divergent.

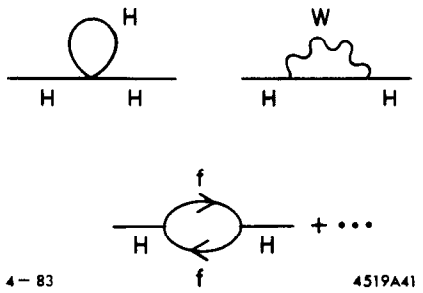

Fig. 54. Examples of loop diagrams which contribute quadratic divergence to the Higgs mass.

This issue is covered very elegantly in the lectures of L. Susskind in these proceedings and we will not take time here to discuss it further. We will consider three ways to avoid the unnaturalness of the Higgs mechanism:

1. Cancel each quadratically divergent diagram uniquely – supersymmetry,
2. Put in a cut-off parameter at a scale of $\sim 10^3$ GeV – technicolor, and
3. Make $SU(2)$ strong at the scale of $\sim 10^3$ GeV – composites of confined fermions.

6.1 SUPERSYMMETRY (SUSY)

In supersymmetry new particles are introduced with couplings such that the quadratic divergences are cancelled graph by graph to all orders. Such a magic cancellation implies a symmetry of nature is at work – in fact a "supersymmetry." The new symmetry is most unfamiliar to us. We are accustomed to symmetries which relate particles of the same spin; multiplets of flavor $SU(3)$, color $SU(3)$, isospin $SU(2)$, electroweak $SU(2) \wedge U(1)$ all contain particles with the same spin. Supersymmetry introduces a high level of uniformity by grouping together in multiplets particles whose spin differ by $\frac{1}{2}$ a unit. Symmetry operations transform fermions into bosons and vice versa. Hence the photon has a SUSY partner with spin $\frac{1}{2}$ called the photino, leptons and quarks have spin zero partners called sleptons and squarks etc., etc. The multiplets of SUSY are shown in Table 8.

Table 8. Supersymmetry Particle Multiplets

	Spin 1	Spin $\frac{1}{2}$	Spin 0
Massless Multiplet	Photon Gluons	Photino Gluino	
Massive Gauge Multiplet	$W^{\pm}$ Z^0, U	Wino, Zino, Goldstino	Shigges
Matter Multiplet		Leptons Quarks	Sleptons Squarks

Unless supersymmetry is broken, we will have a mass degeneracy between the familiar particles and their SUSY partners. This is clearly not the case and hence SUSY must be broken. The mildest way to do this is spontaneously and the simplest scheme was that proposed by Fayet.[48] In Fayet's scheme there is only a single generator, Q_α, which will permit transformations which change the spin by a $\frac{1}{2}$ unit:

$$Q_\alpha|Fermion>=|Boson> \qquad (\alpha = 1,2 \text{ spin index})$$

$$Q_\alpha|Boson>=|Fermion> \quad .$$

Such schemes having only one generator are called "simple" and we will restrict our discussion to such models. (Models having more than one generator are called "extended" models.) In Fayet's model the gauge group is expanded to $SU(2)\wedge U(1)\wedge U(1)'$ which results in a new massive gauge boson which is called U. The spontaneous breakdown of the symmetry is achieved using a pair of complex Higgs doublets. The result is the appearance of charged and neutral scalars (called shigges) as described in Sec. 5.1. There are many schemes for breaking SUSY and each leads to different mass splittings, and hence masses, for the SUSY particles. In Fayet's scheme one obtains bounds for the particle masses and in particular

$$M_{H^{\pm}} \leq 80 GeV/c^2$$

$$M_{H^0} \geq 30 GeV/c^2 \quad .$$

and

$$M_{squarks}, M_{sleptons} \leq \frac{M_{W^{\pm}}}{2} \simeq 40 GeV/c^2 .$$

In this simple model, all the SUSY partners of the fermions have masses below $M_{Z^0}/2$. Other than spin, all members of the same multiplet have the same quantum numbers and hence their couplings to the Z^0 and photon will be the same. The production rates for sfermions are half that of the fermions. (The usual $\frac{1}{4}$ characteristic of scalars is multiplied by two because there are two scalar partners for each fermion.) These comments are modified near threshold by the usual β^3 turn-on for scalar particles.

How do sfermions decay? They decay (see Fig. 55) to their fermion partners plus a photino or goldstino (sleptons) or a photino, gluino or wino (squarks). The photino and goldstino can be thought of as neutrino-like for the purposes of interactions in any detecting device, although in general this statement is not true. This description of SUSY was not intended to be complete or rigorous. The interested reader will find the references in Ref. 49 very complete. However, the preceding discussion suffices to establish how one would search for SUSY particles.

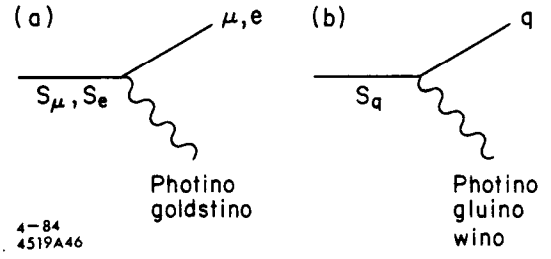

Fig. 55. The decay of sleptons (a) and squarks (b).

Searches for squarks and sleptons can be pursued in the e^+e^- continuum. These scalars will be pair produced with a characteristic $sin^2\theta$ angular distribution and a production rate

$$\sigma(S_q, S_{\bar{q}}) = 3\sigma(S_\ell, S_{\bar{\ell}}) \equiv 3 \cdot \frac{2}{4} \cdot \beta^3 \sigma_{point}$$

and if $\beta = 1$

$$R(S_q, S_{\bar{q}}) = \frac{1}{2} R(q, \bar{q})$$

$$R(S_\ell, S_{\bar{\ell}}) = \frac{1}{2} R(\ell, \bar{\ell})$$

where S_q and S_ℓ refer to the scalar partners of quarks and leptons. For each new squark species, $\delta R = \frac{2}{3}$ or $\frac{1}{6}$ depending on its charge. R is know at PETRA to $\pm 5\%$ (systematic error) or $\simeq 0.2$. Hence it is probable that most or all of the charge $\frac{2}{3}$ squarks have masses above 18.5 GeV/c^2.

Direct searches have been performed for the scalar leptons via the process

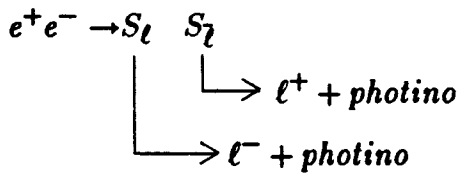

where $\ell = e$ or μ or τ. These searches proceed in an obvious way – one searches for ee, $\mu\mu$ and $\tau\tau$ events in excess of the QED rate. If $\beta \simeq 1$ there would be an increase above QED of $\approx 50\%$ in the yields of these events. One also expects lots of missing energy and momentum. The 95% confidence level limits obtained at PETRA are given in Table 9 which is compiled from the references in Ref. 50. In all these tests the neutral missing particle (photino or goldstino) is assumed to be stable.

Table 9. Mass Limits (95% confidence level) for S_e, S_μ, S_τ (see Ref. 50).

Experiment	Excluded Mass Range (GeV/c^2)		
	Electron	Muon	Tau
CELLO	2 - 16.8	3.3 - 16	6 - 15.3
JADE	< 16	– –	4 - 13
MARK J	– –	3 - 15	M_τ - 14
PLUTO	< 13	– –	– –

The searches described for sleptons involve the assumption that $M_{S_\ell} \leq E_{c..m.}/2$. M. K. Gaillard et al.,[51] have proposed a mechanism whereby one can obtain sensitivity beyond $E_{c.m.}/2$. The process involved in shown in Fig. 56, where the symbol $\tilde{\gamma}$ is used for the photino. Under the assumption that the photino is stable and has a small mass, the e^+ takes up very little transverse momentum and hence continues down the beampipe. The signature is an event with a single electron with substantial energy and

large missing transverse momentum. The cross section for the process is calculated in Ref. 51. One finds that for $E_{c.m.} \simeq 40$ GeV

$$\sigma(S_e\tilde{\gamma}) = 5\%\ \sigma_{point} \qquad \text{for } M_{S_e} = 15\ GeV/c^2$$

$$= .15\%\ \sigma_{point} \qquad \text{for } M_{S_e} = 30\ GeV/c^2\ .$$

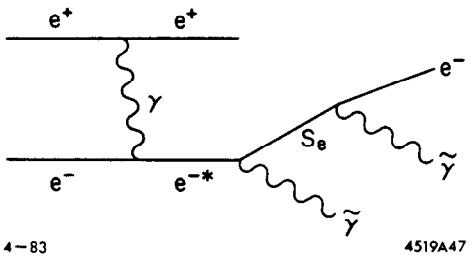

Fig. 56. The process $e^+e^- \to e^+e^-\tilde{\gamma}\tilde{\gamma}$. The e^+ will go perferentially in the forward direction leaving only the e^- in the detector.

For $< \mathcal{L} >= 10^{31}$ this would correspond to an event rate of $\sim$ 100/month and 3/month, respectively. Backgrounds will come from QED processes ($ee\gamma$) where the photon escapes through uninstrumented cracks in the detectors. Suppression of these backgrounds are aided by the fact that the signal has a roughly isotropic angular distribution for the $e^{\pm}$ and the $e^{\pm}$ is energetic. Since the publication of Ref. 51, most of the PEP and PETRA detectors have augmented their hardware so that they will trigger on a single high energy (few GeV) electron. We should expect results from these searches within six to twelve months, with expected mass sensitivity in the range of 20-30 GeV/c^2.

All the tests for charged and neutral Higgs particles given in Secs. 4.3 and 5.1 apply also for the Shiggs particles.

The Z^0 will offer a superb testing ground for SUSY. In Fayet's simple model all the sfermions will have masses below $M_{Z0}/2$ and the Z^0 will be 50% wider than in the standard model. Fayet's model aside, for each new squark, the rate of Z^0 decays will go up by about 5% and for each new charged slepton it will go up by 1.5% ($\beta = 1$ is assumed). The squarks would be heavy and hence detectable using a shape analysis and the sleptons will yield to tests analogous to those described earlier in this section for continuum production. Given the high production rate for Z^0's, these events will easily be seen. The neutrals (photino, goldstino) will be observed in the process

$$e^+e^- \rightarrow \gamma Z^0$$
$$\hookrightarrow \tilde{\gamma}\tilde{\gamma}$$

as described in the neutrino counting experiment of Sec. 5.4.

High energy e^+e^- interactions offer a much wider range of tests than those discussed here. We have ignored the issue of the stability of the neutrals, the detection of the gluino, etc., etc. These can be found in the references or weekly on the preprint shelves. It should be remembered that the simple model of Fayet might be wrong and that the extended models do not necessarily have low lying charged fermions. Supersymmetry is a very attractive theory offering the potential for unifying gravity, QCD and electroweak interactions. Testing SUSY, however, might be very frustrating if the mass scale keeps growing.

6.2 Technicolor Theories – Dynamical Symmetry Breaking

In order to have a theory which is renormalizable, gauge bosons must acquire mass as a result of spontaneous symmetry breaking. In the standard model, this breaking is achieved using the Higgs mechanism. However, it is possible for the gauge interactions themselves to cause spontaneous symmetry breakdown. The class of theories in which this dynamical mechanism is employed is called Technicolor Theories.[52]

In these theories a new set of unbroken, non-Abelian gauge interactions are introduced which become strong at a scale $\Lambda_{TC} \sim 1$ TeV. Technicolor is therefore analogous to QCD with a spectrum of technicolor singlets with masses of ~ 1 TeV. The analogs of the QCD fermions are so called technifermions and the role of the Higgs particles of the standard model are assumed by spin zero bound states of these technifermions. In the minimal technicolor schemes all the light pseudoscalars are eaten by the gauge bosons of the weak interaction. Since we do not have Higgs particles there is no Yukawa mechanism for generating ordinary fermion masses. In technicolor this must be achieved by an additional gauge interaction which couples ordinary fermions to technifermions.

The mass generation scheme in the standard model via Yukawa couplings (a) and the four fermion type interaction in technicolor theories (b) are shown in Fig. 57. Models which include the additional gauge interaction for mass generation are called

extended technicolor (ETC) models. No completely satisfactory model of ETC has emerged as discussed in Susskind's lectures in these proceedings. In the ETC schemes there are more light pseudoscalars than in the minimal model, and after the weak interaction bosons have been given mass, a spectrum of physical scalars (technipions) remain. The number of these technipions depends on the ETC model. However, independent of the model there is an irreducible minimum of four technipions with masses in the 10 GeV/c^2 range. We will call these $P^{\pm}$, P^0 and $P^{0\prime}$. These scalars are analogous to the four light hadrons, $\pi^{\pm}$, π^0 and η^0, of normal color. In addition to the technipions there is a spectrum of technihadrons with masses in the 250-1000 GeV/c^2 range.

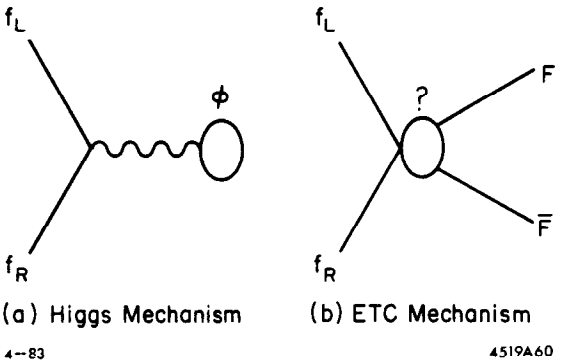

Fig. 57. The generation of fermion masses: (a) via the Higgs field ϕ in the standard model and (b) via the four Fermi type interaction in ETC.

What do we know about the masses of the technipions? There are two contributions to the technipion masses. The first arises from the electroweak interaction and can be calculated in a completely model independent way. The second contribution comes from ETC and is very model dependent. In the absence of ETC, $M_{P^{\pm}} \simeq$ (5-8) GeV/c^2 and $M_{P^0} \equiv 0$. The addition of ETC generates extra mass and typically $M_{P^{\pm}} \leq$ 10-15 GeV/c^2 and $M_{P^0} \leq 5$ GeV/c^2. However there are some ETC models in which $M_{P^{\pm}} \simeq 30$ GeV/c^2.

What about the technipion couplings? In most models the situation is similar to that of charged and neutral Higgs particles – hyperpions like to couple to the heaviest fermion pair available. Since they are scalars their production angular distribution and rate are the same as for H^0, $H^{\pm}$ as discussed in Sec. 4 (H^0) and 5.1 ($H^{\pm}$). In particular the searches for $H^{\pm}$ described in Sec. 5.1 (see Fig. 46) apply equally well for $P^{\pm}$. Hence it is very unlikely that $M_{P^{\pm}} \leq 15$ GeV/c^2 and this eliminates a large class of technicolor models. As PETRA raises its energy and, assuming that no scalars

are found, technicolor is becoming a less likely scenario. By the end of 1983, PETRA experiments will have sensitivity to $M_{P\pm} \leq 22$ GeV/c^2.

Supposing that a charged scalar is found. Is it a technipion or a Higgs? Given the freedom in the models, it will be very difficult to distinguish these two possibilities.[53] However, if we assume that either the standard model or technicolor is correct but not both, then the neutral scalars could provide a means for separating these two options. We recall from Sec. 4 the discussion of the processes $Z^0 \to H^0 Z^{0*} \to H^0 \ell^+ \ell^-$ and $e^+e^- \to Z^{0*} \to Z^0 H^0$. These processes involved the coupling $Z^0 Z^0 H^0$ which is large in the standard model. However for technicolor the $Z^0 Z^0 P^0$ coupling is zero to first order and the analogous decays involving P^0 particles occur at an exceedingly low rate.[53] Typically one finds that the rates for the channels involving P^0's are about 10^{-4} times smaller than those involving H^0's. Hence if we observe these processes, then we confirm the standard model. If no such processes are seen but a charged scalar has been found, then the most likely scenario is that the standard model is wrong and technicolor could be correct.

The searches for technihadrons will require LEP III and the high energy colliding linac machines.

6.3 Composite Models; Strong $SU(2)$

Another solution to the gauge hierarchy problem is offered by the model of Abbott and Farhi[54] in which the weak interactions are the result of the composite nature of quarks and leptons. In this model the $SU(2)$ is strong and hence confining at the scale of the weak interactions, $\mathcal{G}_F^{-\frac{1}{2}} \simeq 300$ GeV. This procedure is analogous to QCD in which the confining scale is at a few hundred MeV. In the same sense that QCD offers a sensible way to set a mass scale, the strong $SU(2)$ theory does too and the gauge hierarchy problem is avoided. The composite model retains the gauge structure of the standard model namely $SU(3) \wedge SU(2) \wedge U(1)$. It contains a complex doublet of Higgs fields, but the scalar potential is adjusted so that no spontaneous symmetry breaking occurs. The particle content is the same as in the standard model – left-handed doublets and right-handed singlets. Since the right-handed fermions are singlets of $SU(2)$ they are not confined and hence are the right-handed quarks and leptons. However, the left-handed fermions are confined at the scale $\mathcal{G}_F^{-\frac{1}{2}}$ and the familiar left-handed fermions must be constructed from these confined particles. The

absence of spontaneous symmetry breaking implies that $U(1)$ and $SU(2)$ are not mixed and hence $U(1)$ becomes the $U(1)$ of electromagnetism.

In analogy with QCD, we expect a rich spectrum of particles, most of them with masses $\simeq$ 300 GeV. There are some bound states with light masses and these are the left-handed quarks and leptons. These particles are constructed out of bound states of the left-handed confined fermions and the scalars mentioned above. This generates particles with the correct quantum numbers but they are massless. Yukawa couplings are used to generate mass for the quarks and leptons and in this way the full quark and lepton spectrum of the standard model is recovered.

The weak interaction Lagrangian in this theory is

$$\mathcal{L} = \frac{4\mathcal{G}_F}{\sqrt{2}}\left\{J_\mu^+ J_\mu^- + (J_\mu^3)^2\right\} + \frac{4\mathcal{G}_F}{\sqrt{2}}\,\xi\,(J_\mu^0)^2$$

where $\vec{J}_\mu = (J^+, J^-, J^3)$ is the weak isovector current and J_μ^0 is the weak isoscalar current. Since no evidence for the latter current exists, ξ is assumed, without any justification, to be <0.05. The standard model weak interaction Lagrangian is

$$\mathcal{L}_{SM} = \frac{4\mathcal{G}_F}{\sqrt{2}}\left\{J_\mu^+ J_\mu^- + (J_\mu^3 - sin^2\theta_W J_{em})^2\right\} \ .$$

How do we account for the difference and hence make the composite model Lagrangian consistent with the low energy data? The solution lies in the observation that, because of the composite nature of the fermions, they possess electric (and magnetic) form factors. When one adds in the contribution from the interaction of this charge distribution and the electromagnetic interaction (γ's), one can obtain consistency with the low energy data. The parameter $sin^2\theta_W$ in this model has nothing to do with electroweak mixing. Rather it measures the strength of the mixing between a photon and one of the vector mesons of strong $SU(2)$. The data can be fit if this mixing parameter takes on a value of 0.23. This is a very large mixing when compared with the comparable QCD situation where the photon-rho mixing is 0.02. The strong $SU(2)$ theory does not explain the large mixing; the value is taken to ensure that the experimental data can be fit. Also it is odd that while the electric form factor is large the magnetic form factor must be kept small so as not to develop too large a muon magnetic moment.

Following the discussion above, this model can describe the low energy data. However, there is no narrow Z^0 in this model. If there is a narrow Z^0 in the 100 GeV/c^2

mass range then this model is wrong. If there is no Z^0, and this model becomes a candidate for the standard model, we would have to search for the particle spectrum associated with the strong scale at $\mathcal{G}_F^{-\frac{1}{2}}$ (cf hadrons of QCD). There will be particles with masses $\geq$ 250 GeV/c^2. In addition (ala π's in QCD) there will be some vector mesons with masses in the 100-200 GeV/c^2 range. They will not be easy to find because they will decay strongly and can be expected to have widths on the order of 20-30 GeV. The best signature would come from the fact that these strong $SU(2)$ decays will treat quarks and leptons democratically (aside from the 3:1 advantage from color) and hence one will see a lot of leptons in the decays. One would need to be running at LEP II and LEP III with a device which had good lepton/hadron rejection so that a clean measurement of R_e or R_μ could be made. This possibility is discussed[55] by DeRugula in a delightful article on "glints." The study of the high mass spectrum will require the colliding linac machines.

We have discussed a model in which the quarks and leptons are composite. What experimental evidence do we have for the size of fermions? Since photons couple to charge they make an excellent probe of the size of fermions. This can be done using measurements of the processes

$$e^+e^- \rightarrow f\bar{f}$$

where $f = e, u, \tau, q$. The data at PETRA have been fit assuming that the pointlike QED cross section is modified by a form factor of the type

$$F^{\pm} = 1 \mp \frac{q^2}{q^2 - \Lambda_{\pm}^2} \quad .$$

Table 10 shows the 95% confidence level lower limits for $\Lambda_{\pm}$. These results are taken from Ref. 18.

Table 10. 95% Confidence Level Lower Limits for $\Lambda_{\pm}$ (GeV)

	e		μ		τ		q	
	Λ^+	Λ^-	Λ^+	Λ^-	Λ^+	Λ^-	Λ^+	Λ^-
CELLO	83	85	–	–	139	120	–	–
JADE	112	106	142	126	111	93	–	–
MARK J	128	161	194	153	126	116	190	285
PLUTO	80	234	107	101	79	63	–	–
TASSO	140	296	127	136	104	189	–	124

We may conclude that fermions are pointlike down to $\sim 10^{-16}$ *cm*. As we go to higher energies we must continue these measurements to probe larger composite mass scales.

7. Summary and Conclusions

We have discussed how we can continue to test the standard model using e^+e^- interactions at energies beyond those presently available. We have seen that the machines which we will have available in the next ten years will permit us to make many important and decisive tests of the standard model. We have investigated how we can test theories which go beyond the standard model. Some of these theories involve minor modifications of the standard model, others were much more radical. We saw that these studies are done in the continuum, at toponium and at the Z^0. Rather than summarize the important searches in words, we have chosen to provide the reader with a reminder in the form of Table 11. The key for this table is $E \equiv E_{c.m.}$, a cross indicates that the search is not possible, a check indicates that it is, and no entry means that an entry is not applicable or not interesting.

How are we situated with respect to Table 11? Figure 58 summarizes the available energy of e^+e^- high energy machines as a function of calendar year. Toponium and the Z^0 are vital to our searches. Z^0 factories will soon exist in both the U.S.A. and Europe and by 1988 there should be five or six good detectors running at the Z^0. If $M_t < M_{Z^0}/2$, then toponium can be studied at one or some of PETRA/TRISTAN/SLC/LEP. The region from 100-250 GeV is covered by LEP on a time scale estimated to be the early 1990's.

But we saw lots of options for thresholds above $\mathcal{G}_F^{-\frac{1}{2}} \simeq 300$ GeV. Supersymmetry, technicolor, composite models are but a few of these options. This is clearly the new frontier and every effort must be made to accelerate the availability of the colliding linacs. If we look at Fig. 58 we find that, to very good approximation, the entries lie on a straight line. If we extrapolate this line to $E_{c.m.} = 500$ GeV (1000 GeV) we find ourselves in the year 2000 (2005). Hopefully we can prove that the present linear relationship is not a universal law of nature and that the frontier machines can be built and operated in this century.

Table 11. Summary of Searches Discussed in These Lectures.

	Continuum	Z^0	Toponium
Top	$E > 38$ GeV	√	√
Z^0	$E > 38$ GeV lower limit on M_{Z^0}	√	×
$W^\pm$	$E > 2M_W$	×	×
H^0	$E > M_{Z^0}$	√	√
Gluon	maybe, $E > 38$ GeV	√	√
Free quark	All E	√	√
$H^\pm$	$M_H < M_t$	×	√; $M_H < M_t$
Multiple Z's	M_Z, $E > M_{Z^0}$	√ (M_1)	×
New Generations:			
$L^\pm$	√	√	√
$Q = -\frac{1}{3}$	maybe, rate limited	√	
ν's	$100 < E < 110$ GeV	√	
SUSY:			
S_q	√	√	√
S_L	√	√	√
Technicolor:			
$P^\pm$	same as $H^\pm$		
P^0	$E > M_{Z^0}$ (*)	√ (*)	√
Technihadron	$E > 200$ GeV	×	×
$SU(2)_{strong}$	$E > 100$ GeV $E > 250$ GeV	√ (*)	
Composites	All E		

*Null result expected.

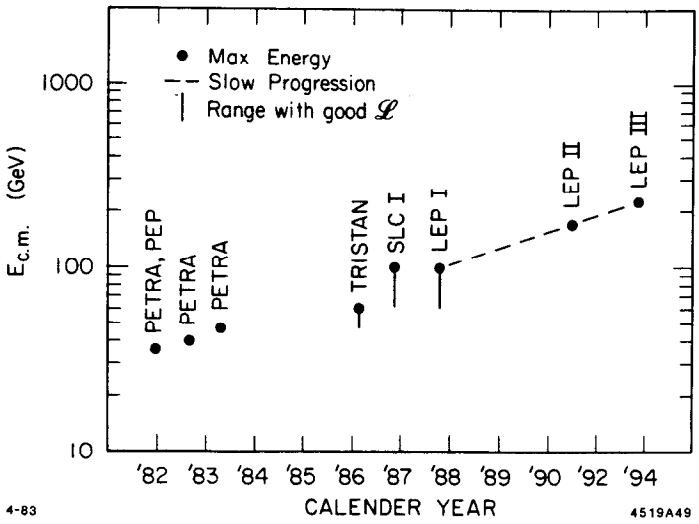

Fig. 58. The march towards the final frontier! The available energy for the e^+e^- machines as a function of calendar year. In the case of the new machines a range of expected good luminosity is shown.

We should remember that we could arrive at $\sim$ 200 GeV and the standard model might still be the best description of nature which we have. What then? The sceptics will say that there is no good reason to push further for surely only Bedouins like deserts! Well the response to those sceptics is, "What self-respecting Bedouin would resist an oasis?" The only way to demonstrate that there is nothing new happening beyond the frontier is to cross it!

e^+e^- interactions at very high energies offer the potential for wide ranging tests of current high energy theories. The next ten years should prove to be very exciting indeed.

Acknowledgements

The author would like to thank Fred Gilman for his guidance in choosing the structure and format of these lectures. The author would also like to thank Peter Zerwas for many helpful and illuminating discussions. In addition the author wishes to than Bette-Jane Ferandin for her tireless effort in the preparation of this document.

REFERENCES

1. G. A. Voss, Proceedings of the 1981 International Symposium on Lepton and Photon Interactions at High Energies, Bonn, 1981, p. 926.
2. CERN Courier, Vol. 22 (10), p. 411 and p. 415 (1982).
3. S. Ozaki, Proceedings of the 1981 International Symposium on Lepton and Photon Interactions at High Energies, Bonn, 1981, p. 935.
4. SLAC Linear Collider Conceptual Design Report, SLAC-299 (June 1980); B. Richter, SLAC-PUB-2854 (1981).
5. (a) C. Y. Prescott, SLAC-PUB-2854 (1981). (b) Proceedings of the SLC Workshop, SLAC-247 (March 1982).
6. See for instance ECFA 81/54, General Meeting on LEP Villars-sur-Ollon, Switzerland, June 1981 and references therein.
7. ECFA 81/54, General Meeting on LEP Villars-sur-Ollon, Switzerland, June, 1981, p. 132.
8. U. Amaldi, Proceedings of the 1981 International Symposium on Lepton and Photon Interactions at High Energies, Bonn, 1981, p. 944.
9. J. Kim et al., Reviews of Modern Physics 53, 211 (1981).
10. W. Marciano and A. Sirlin, Proceedings of the Cornell Z^o Theory Workshop, February 1981, p. 40.
11. A. Buras, Phys. Rev. Lett. 46, 1354 (1981).
12. The aplanarity is defined in the sphericity tensor analyses: J. D. Bjorken and S. J. Brodsky, Phys. Rev. D 1, 1416 (1970). For the use of aplanarity as described here see for instance TASSO collaboration, Phys. Lett. 86B, 243 (1979).
13. For a review of the PETRA measurements see J. Bürger, Proceedings of the 1981 International Symposium on Lepton and Photon Interactions at High Energies, Bonn, 1981, p. 126.
14. M. Dine and J. Sapirstein, Phys. Rev. Lett. 43, 668 (1979); K. G. Chetyrkin et al., Phys. Lett. 85B, 277 (1979); W. Celmaster and R. J. Gonsalves, Phys. Rev. Lett. 44, 560 (1980).
15. J. Dorfan, Z. Phys. 17, 349 (1981).
16. G. J. Tarnopolsky, SLAC-PUB-2842 (1981).
17. The error in $sin^2\theta_W$ is assumed to be one order of magnitude smaller than its present value, since the precision will be achieved by the measurement of the Z^o mass.

18. See for instance J. G. Branson, Proceedings of the 1981 International Symposium on Lepton and Photon Interactions at High Energies, Bonn, 1981, p. 279.

19. F. Wilczek, Phys. Rev. Lett. 39, 1304 (1978).

20. J. P. Leveille, Proceedings of the Cornell Z^0 Theory Workshop, February 1981, p. 242.

21. J. D. Bjorken, SLAC-198 (1976).

22. R. N. Cahn et al., Phys. Lett. 82B, 117 (1979).

23. S. L. Glashow et al., Phys. Rev. D 18, 1724 (1978).

24. P. Söding, AIP Conference Proceedings, No. 81, 107 (1981).

25. W. Braunschweig, Proceedings of the 1981 International Symposium on Lepton and Photon Interactions of High Energies, Bonn, 1981, p. 68.

26. J. Dorfan, Proceedings of the SLAC Summer Institute on Particle Physics, July 1981; SLAC-PUB-2813 (1981).

27. Examples of three jet algorithms are: TRIPLICITY - S. Brandt and H. Dahmen, Z. Phys. C1, 61 (1979). TRIJETTINESS - S. L. Wu and G. Zobernig, Z. Phys. C2, 207 (1979). CLUSTER ALGORITHM - J. Dorfan, Ref. 15, ibid.

28. J. Ellis and I. Karliner, Nucl. Phys. B148, 141 (1979).

29. R. Hollebeek, Proceedings of the 1981 International Symposium on Lepton and Photon Interactions of High Energies, Bonn, 1981, p. 1.

30. J. K. Bienlien, Proceedings of the 1981 International Symposium on Lepton and Photon Interactions of High Energies, Bonn, 1981, p. 190.

31. (a) R. D. Shamberger, Proceedings of the 1981 International Symposium on Lepton and Photon Interactions of High Energies, Bonn, 1981, p. 217. (b) A. Silverman, Proceedings of the 1981 International Symposium on Lepton and Photon Interactions of High Energies, Bonn, 1981, p. 138.

32. G. Preparata et al., Phys. Rev. Lett. 47, 891 (1981); G. Preparata, Proceedings of Physics in Collision I, 1981, p. 53; G. Preparata et al., BARI/GT/81-16.

33. K. Koller et al., SLAC-PUB-2858 (1982).

34. O. Nachtman et al., HD-THEP-82-9 (1982).

35. G. Körner et al., Nucl. Phys. B185, 365 (1981).

36. JADE Collaboration: W. Bartel et al., DESY 82-086 (1982).

37. See Ref. 25, page 87, MARK J results.

38. B. Lohr et al., SLAC-PUB-2983 (1982).

39. G. S. Larue et al., Phys. Rev. Lett. 38, 1011 (1977); Phys. Rev. Lett. 42, 142 (1979); Phys. Rev. Lett. 46, 967 (1981).

40. MARK II Collaboration: C. A. Blocker et al., Phys. Rev. Lett. 49, 517 (1982). CELLO Collaboration: H. J. Behrend et al., DESY 82-021 (1982). JADE Collaboration: W. Bartel et al., Phys. Lett. 114B, 211 (1982). MARK J Collaboration: A. Adeva et al., LNS Technical Report No. 125 (1982). TASSO Collaboration: M. Althoff et al., DESY 82-069 (1982).

41. E. H. De Groot et al., Z. Phys. C5, 127 (1980). This reference discusses the general question of $SU(2) \wedge U(1) \wedge G$.

42. V. Barger et al., Phys. Rev. D 25, 1384 (1982).

43. A. De Rugula et al., Annals of Phys. 109, 242,258 (1977).

44. G. Kane, UMHE 80-18 (1980); G. Kane and M. Peskin, UMHE 81-51 (1981).

45. M. Peskin and S.-H. H. Tye, Proceedings of the Cornell Z^0 Theory Workshop, CLNS-81-485 (1981).

46. J. D. Bjorken, SLAC-PUB-2195 (1978).

47. G. Barbiellini et al., Phys. Lett. 106B, 414 (1981).

48. P. Fayet, Phys. Lett. 69B, 489 (1977).

49. Review articles include: P. Fayet, "Supersymmetry, Particle Physics, and Gravitation," Proceedings of the Europhysics Study Conference on "Unification of the Fundamental Interactions," Erice, Sicily, March 17-24, 1980 and CERN preprint TH-2864, which emphasizes theoretical aspects of spontaneously broken supersymmetry; G. R. Farrar, Proceedings of the International School of Subnuclear Physics, Erice (Italy), August 1978, which emphasizes low energy phenomenological implications; and P. Fayet and S. Ferrara, Phys. Rep. 32C, 249 (1977), which surveys the whole field of supersymmetry as it existed in 1977.

50. JADE Collaboration: D. Cords, Proceedings of the XXth International Conference on High Energy Physics, Madison, 1980. MARK J Collaboration: D. P. Barber et al., Phys. Rev. Lett. 45, 1904 (1980). PLUTO Collaboration: H. Spitzer, Proceedings of the XIth Rencontre de Moriond, ed. Tran Than Van, Les Arcs, 1980, and DESY 80-43 (1980). CELLO Collaboration: H.-J. Berend et al., DESY 82-021 (1982). New results have also been published by JADE Collaboration: W. Bartel et al., DESY 82-023 (1982). MARK J Collaboration: B. Adeva et al., MIT/LNS 125 (1982).

51. M. K. Gaillard et al., Phys. Lett. 116B, 279 (1982).

52. S. Weinberg, Phys. Rev. D 19, 1277 (1979); L. Susskind, Phys. Rev. D 20, 2619 (1979); K. Lane and M. Peskin, Proceedings of the 1980 Rencontre de Moriond, ed. J. Tran Than Van; E. Eichten, Proceedings of the 1980 Vanderbilt e^+e^- Conference; E. Farhi and L. Susskind, CERN preprint TH-2975; P. Sikivie, Varenna Lectures (1980).

53. A. Ali and M. A. B. Beg, Phys. Lett. 103, 376 (1981).

54. L. F. Abbott and E. Farhi, Phys. Lett. 101B, 69 (1981); Nucl. Phys. B189, 547 (1981).

55. A. De Rugula, Phys. Lett. 96B, 279 (1980).